### 2.6. Blood-to-retina [$^3$H]adenosine transport studies

The apparent retinal uptake clearance of [$^3$H]adenosine ($K_{in,\ retina}$) [μL/(min g retina)] from the circulating blood to the retina was determined by integration plot analysis as described previously [15]. Briefly, the rats were anesthetized with an intramuscular injection of ketamine-xylazine (1.22 mg xylazine and 125 mg ketamine/kg) and then [$^3$H]adenosine (12 μCi/head) was injected into the femoral vein. After collection of blood samples, rats were decapitated, and the retinas were removed. The retinas were dissolved in 2 N NaOH and subsequently neutralized. The radioactivity was measured in a liquid scintillation counter. As an index of the retinal distribution characteristics of [$^3$H]adenosine, the apparent retina-to-plasma concentration ratio ($V_d$) was used. This ratio [$V_d(t)$] (mL/g retina) was defined as the amount of [$^3$H] per gram retina divided by that per milliliter plasma, calculated over the time-period of the experiment ($t$). The apparent blood-to-plasma concentration ratio ($R_B$) was also measured to examine the [$^3$H]adenosine uptake into the blood cells. The $K_{in,\ retina}$ can be described by following Eq. (2):

$$V_d(t) = K_{in,\ retina} \times AUC(t)/C_p(t) + V_i \quad (2)$$

where AUC($t$) (dpm min/mL), $C_p(t)$ (dpm/mL), and $V_i$ (mL/g retina) represent the area under the plasma concentration time curve of [$^3$H]adenosine from time 0 to $t$, the plasma [$^3$H]adenosine concentration at time $t$, and the rapidly equilibrated distribution volume of [$^3$H]adenosine in the retina, respectively. $V_i$ is usually comparable with the vascular volume of the retina.

The inhibitory effect of nucleosides on the blood-to-retina transport of [$^3$H] adenosine was evaluated by the retinal uptake index (RUI) method [20,21]. Briefly, the rats were anesthetized with an intramuscular injection of ketamine-xylazine and then 200 μL of injection solution was injected into the common carotid artery. The injection solution consisted of Ringer–HEPES buffer (141 mM NaCl, 4 mM KCl, 2.8 mM $CaCl_2$, 10 mM HEPES, pH 7.4) which contained both a test compound, 10 μCi [$^3$H]adenosine or D-[1-$^3$H(N)]mannitol ([$^3$H]D-mannitol, 17 Ci/mmol, PerkinElmer Life Sciences, Boston, MA), and a reference compound, 0.1 μCi n-[1-$^{14}$C]butanol ([$^{14}$C]n-butanol, 2 mCi/mmol, American Radiolabeled Chemicals, St. Louis, MO), in the presence or absence of inhibitors. Rats were decapitated at 15 sec after injection, and the retina was removed. The retina was dissolved in 2 N NaOH and subsequently neutralized. The radioactivity was measured in a liquid scintillation counter. In this study, the RUI value was used as an index of the retinal distribution characteristics of [$^3$H] adenosine and can be described by following Eq. (3):

$$RUI = \frac{[^3H]/[^{14}C](\text{dpm in the retina})}{[^3H]/[^{14}C](\text{dpm in the injection solution})} \times 100 \quad (3)$$

### 2.7. Data analysis

Unless otherwise indicated, all data represent means±S.E.M. An unpaired, two-tailed Student's $t$-test was used to determine the significance of differences between two groups. Statistical significance of differences among means of several groups was determined by one-way analysis of variance followed by the modified Fisher's least-squares difference method.

## 3. Results

### 3.1. Expression of nucleoside transporters in TR-iBRB2 cells

RT-PCR analysis was performed to examine the expression of ENT and CNT mRNAs in the rat retina and TR-iBRB2 cells. As shown in Fig. 1, the expression of ENT1, ENT2, CNT1, and CNT2 in the retina was detected at 431, 562, 479, and 298 bp, respectively. Of the four transporters, the expression of ENT1, ENT2, and CNT2 was also detected in TR-iBRB2 cells. The expression of CNT3 was not detected in the retina, however, and only a minor band of CNT3 was detected in TR-iBRB2 cells.

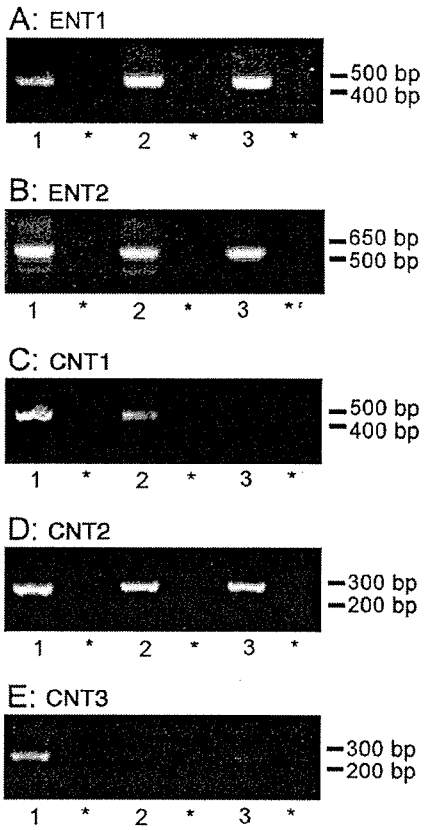


Fig. 1. RT-PCR analysis of ENT1 (A), ENT2 (B), CNT1 (C), CNT2 (D), and CNT3 (E) expression in TR-iBRB2 cells. Lane 1: positive control; lane 2: rat retina; lane 3: TR-iBRB2 cells. *: in the absence of reverse transcriptase for the respective left-hand lane. Rat brain (ENT1 and ENT2), kidney (CNT1), liver (CNT2), and small intestine (CNT3) were used as positive controls.

### 3.2. [$^3$H]Adenosine uptake by TR-iBRB2 cells

To analyze the kinetics and characteristics of adenosine transport at the inner BRB, [$^3$H]adenosine uptake was investigated using TR-iBRB2 cells as an in vitro model of the inner BRB. The time-courses of [$^3$H]adenosine uptake by TR-iBRB2 cells in the presence or absence of $Na^+$ are shown in Fig. 2. [$^3$H]Adenosine uptake increased linearly for at least 10 min. $Na^+$-free conditions had no effect on [$^3$H]adenosine uptake until 10 min, supporting the hypothesis that [$^3$H] adenosine uptake by TR-iBRB2 cells is predominantly mediated by ENT.

Fig. 3 shows the concentration-dependent uptake of adenosine by TR-iBRB2 cells. The Eadie–Scatchard plot (Fig. 3, inset) gave a single straight line, indicating that one saturable process was involved in adenosine uptake by TR-iBRB2 cells. Kinetic analysis of the uptake data using Eq. (1) and nonlinear least-squares regression analysis, gave a $K_m$ of 28.5±2.2 μM and a $J_{max}$ of 814±45 pmol/(min mg protein) (mean±S.D.).

The inhibition study was performed to characterize the [$^3$H] adenosine transport system in TR-iBRB2 cells (Table 1). Of the nucleosides studied, adenosine, inosine, uridine, and thymidine,

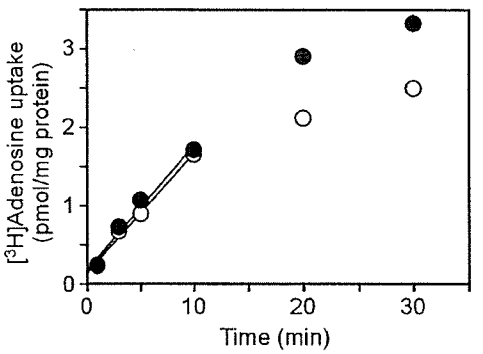


Fig. 2. Time-course of [$^3$H]adenosine uptake by TR-iBRB2 cells. The [$^3$H] adenosine (14 nM) uptake was performed at 37 °C in the presence (closed circle) or absence (open circle) of $Na^+$. Each point represents the mean±S.E.M. ($n$=4). The error bar is smaller than the size of the symbol.

at a concentration of 2 mM, inhibited [$^3$H]adenosine uptake by more than 60%, while guanosine and cytidine, at a concentration of 2 mM, partially inhibited it by up to 40%. [$^3$H] Adenosine uptake was also inhibited by nucleobases, such as 2 mM adenine and 2 mM hypoxanthine, by 41% and 28%, respectively. The $Na^+$-independent nucleoside transport systems can be classified according to their sensitivity to NBMPR and dipyridamole [8]. NBMPR and dipyridamole, at a concentration of 100 nM, did not inhibit [$^3$H]adenosine uptake, while NBMPR (10 and 100 μM) and dipyridamole (1 and 10 μM) produced more than 50% inhibition. These results represent NBMPR- and dipyridamole-insensitive transport of adenosine in TR-iBRB2 cells.

### 3.3. Expression levels of ENT1 and ENT2 in TR-iBRB2 cells

To determine the dominant ENT in TR-iBRB2 cells, quantitative real-time PCR analysis was performed to quantify the mRNA expression levels of ENT1 and ENT2 in TR-iBRB2 cells (Fig. 4). The degree of mRNA expression compensated with β-actin, for ENT1 and ENT2 was $3.27\pm0.29\times10^{-3}$ and $1.81\pm0.33\times10^{-2}$, respectively. Accordingly, the expression of ENT2 mRNA was 5.5-fold greater than that of ENT1 in TR-iBRB2 cells.

Table 1
Effect of several inhibitors on [$^3$H]adenosine uptake by TR-iBRB2 cells

| | Inhibitors | Percentage of control |
|---|---|---|
| | Control | 100±1 |
| 2 mM | Adenosine | 4.75±0.13** |
| 2 mM | Inosine | 20.9±0.3** |
| 2 mM | Uridine | 35.7±1.5** |
| 2 mM | Thymidine | 24.4±0.6** |
| 2 mM | Guanosine | 60.3±1.7** |
| 2 mM | Cytidine | 70.5±3.4** |
| 2 mM | Adenine | 59.2±4.4** |
| 2 mM | Hypoxanthine | 71.8±3.8** |
| 100 nM | Nitrobenzylmercaptopurine riboside (NBMPR) | 86.3±1.9* |
| 10 μM | NBMPR | 43.9±1.8** |
| 100 μM | NBMPR | 10.5±0.6** |
| 100 nM | Dipyridamole | 92.0±1.4 |
| 1 μM | Dipyridamole | 42.3±1.7** |
| 10 μM | Dipyridamole | 8.14±0.16** |

[$^3$H]Adenosine uptake (14 nM) was performed in the absence (control) or presence of 2 mM inhibitors at 5 min and 37 °C. Each value represents the mean±S.E.M. ($n$=4–12).
* $P<0.05$ significantly different from the control.
** $P<0.001$, significantly different from the control.

### 3.4. Blood-to-retina transport of [$^3$H]adenosine

The in vivo blood-to-retina influx transport of adenosine from the circulating blood to the retina through the BRB was evaluated by an integration plot analysis after intravenous administration of [$^3$H]adenosine and application of the RUI method using rats. The $K_{in,\ retina}$ of [$^3$H]adenosine was found to be 25.8±0.7 μL/(min g retina) (mean±S.D.) from the slope of the integration plot (Fig. 5A). The $K_{in,\ retina}$ includes

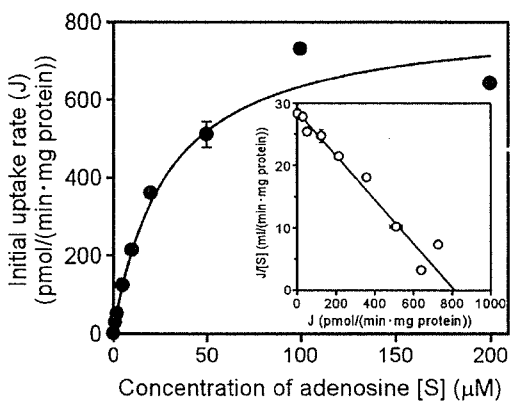


Fig. 3. Concentration-dependence of adenosine uptake by TR-iBRB2 cells. The [$^3$H]adenosine (14 nM) uptake was performed at 5 min and 37 °C. Each point represents the mean±S.E.M. ($n$=4). Data were subjected to Michaelis–Menten and Eadie–Scatchard analyses (inset). The $K_m$ is 28.5±2.2 μM and $J_{max}$ is 814±45 pmol/(min mg protein) (mean±S.D.).

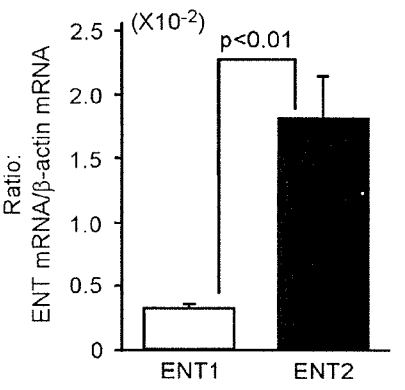


Fig. 4. The amount of ENT1 and ENT2 mRNA in TR-iBRB2 cells. The amount of ENT1 and ENT2 mRNA in TR-iBRB2 cells was determined by quantitative real-time PCR analysis. Data are the mean±S.E.M. ($n$=4). The quantity of ENT1 mRNA relative to β-actin mRNA (ENT1/β-actin) in TR-iBRB2 cells was $3.27\pm0.29\times10^{-3}$, and that of ENT2 mRNA (ENT2/β-actin) was $1.81\pm0.33\times10^{-2}$.

the apparent uptake clearance into the retinal blood (e.g. erythrocytes) as well as the apparent influx clearance across the BRB. In the case of adenosine, the apparent uptake clearance into the retinal blood cannot be ignored, since the $R_B$ of [$^3$H]adenosine was increased with a slope of 0.0882 ± 0.0149 $min^{-1}$ (mean±S.D.) (Fig. 5B). This behavior of adenosine is consistent with a previous report showing that adenosine accumulates in erythrocytes [22]. The vascular volume in the retina was found to be 0.167±0.010 mL/g retina from the $V_i$ of [$^3$H]adenosine (Fig. 5A). By multiplying the slope of the $R_B$ increment and the vascular volume in the retina, the apparent uptake clearance into retinal blood found to be 14.7±3.3 μL/(min g retina). Therefore, the apparent influx clearance across the BRB was found to be 11.1±4.1 μL/(min g retina). The influx transport of adenosine across the BRB was also supported by the fact that the estimated RUI value of [$^3$H]adenosine was greater than that of [$^3$H]D-mannitol (Table 2). Moreover, adenosine and thymidine at a concentration of 2 mM significantly decreased the RUI value of [$^3$H]adenosine to 70% and 75%, respectively, while 2 mM cytidine had no effect. These results confirm the carrier-mediated transport of adenosine from the blood to the retina across the BRB.

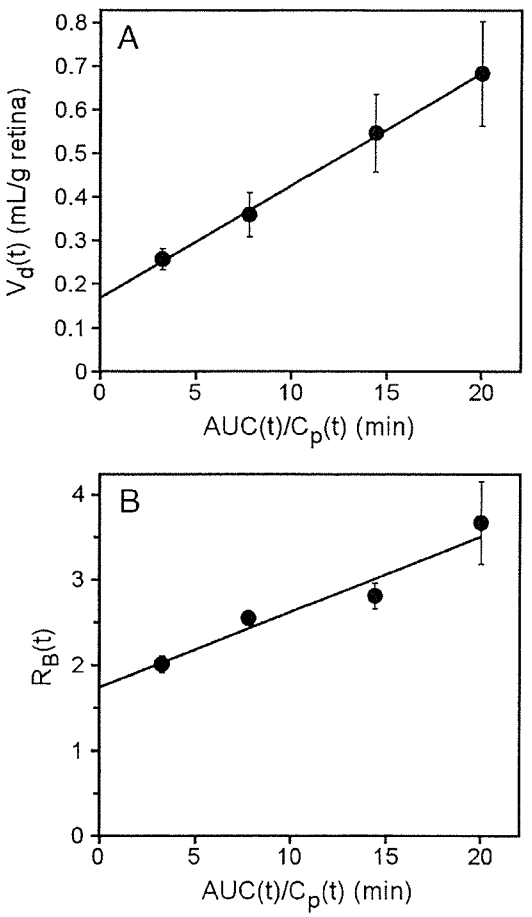


Fig. 5. Integration plot of the initial uptake of [$^3$H]adenosine by the retina (A) and blood-to-plasma concentration ratio ($R_B$) (B) after intravenous administration. [$^3$H]Adenosine (12 μCi/head) was injected into the femoral vein. Each point represents the mean±S.E.M. ($n$=3–4).

Table 2
Retinal uptake index (RUI) of [$^3$H]adenosine and [$^3$H]D-mannitol

| Compounds | Inhibitors | RUI (%) | Percentage of control |
|---|---|---|---|
| [$^3$H]Adenosine | | 32.3±2.8 | 100±9 |
| | Adenosine | 22.7±3.2* | 70.4±10.0* |
| | Thymidine | 24.1±2.4* | 74.7±7.3* |
| | Cytidine | 35.0±1.7 | 108±5 |
| [$^3$H]D-Mannitol | | 11.6±1.4 | |

A test compound, [$^3$H]adenosine or [$^3$H]D-mannitol (10 μCi/head), and a reference compound, [$^{14}$C]n-butanol (0.1 μCi/head), were injected into the common carotid artery in the presence or absence of 2 mM inhibitors. Each value represents the mean±S.E.M. ($n$=3–9).
* $P$<0.05 significantly different from the control.

## 4. Discussion

The present study shows that the BRB is able to transport [$^3$H]adenosine (Fig. 5). The nucleoside transporters are classified as an $Na^+$-independent ENT and an $Na^+$-dependent CNT. TR-iBRB2 cells, an in vitro model of the rat inner BRB, express both ENT and CNT mRNAs (Fig. 1), however, $Na^+$-independent uptake of [$^3$H]adenosine by TR-iBRB2 cells (Fig. 2) suggests that ENT is predominantly involved in the adenosine transport in TR-iBRB2 cells.

ENTs can be further sub-divided into two isoforms according to their sensitivity to NBMPR [8]. The NBMPR-sensitive (*es*) transporter, ENT1, is blocked by less than 100 nM NBMPR ($IC_{50}$=4.6 nM) [23] while the NBMPR-insensitive (*ei*) transporter, ENT2, requires more than 1 μM NBMPR to inhibit nucleoside transport [23]. Although both ENT1 and ENT2 have a variety of nucleoside substrates, ENT2 exhibits a lower affinity for guanosine and cytidine than ENT1 [24]. Moreover, only ENT2 is capable of low affinity transport of nucleobases, such as adenine and hypoxanthine [25]. In TR-iBRB2 cells, [$^3$H]adenosine uptake was not inhibited by NBMPR at 100 nM, but was inhibited at 10 and 100 μM (Table 1). [$^3$H]Adenosine uptake by TR-iBRB2 cells was inhibited by nucleosides, however, the degree of inhibition by adenosine, inosine, uridine, and thymidine was greater than that produced by guanosine and cytidine. In addition to nucleosides, [$^3$H]adenosine uptake by TR-iBRB2 cells was partly inhibited by nucleobases, such as adenine and hypoxanthine. Such forms of inhibition in TR-iBRB2 cells are consistent with ENT2 rather than ENT1. Moreover, quantitative real-time PCR analysis clearly demonstrated that ENT2 is predominantly expressed in TR-iBRB2 cells (Fig. 4). In the light of these findings, adenosine transport in TR-iBRB2 cells is most likely mediated by ENT2.

[$^3$H]Adenosine uptake by TR-iBRB2 cells was not inhibited by dipyridamole at 100 nM, but was inhibited at 1 and 10 μM (Table 1). Dipyridamole is also known to be a useful inhibitor for distinguishing human ENT1 from ENT2, since it blocks human ENT1 and ENT2 with a $K_i$ of 5 nM and 360 nM, respectively [24]. However, in the rat, there are some contradictory reports about the ability of dipyridamole to inhibit rat ENT-mediated transport. The inhibitory effect

observed in human ENT is similar to that in rat C6 glioma cells [26] and rat brain microvascular endothelial cells [27,28] as well as the TR-iBRB2 cells in this study, while 1 μM dipyridamole had no effect on transport activity in recombinant rat ENT1 and ENT2 expressed in *Xenopus* oocytes [23]. These observations indicate that dipyridamole is an effective inhibitor of ENT2-mediated transport in the case of TR-iBRB2 cells, although its inhibitory effect seems to depend on the cell type and preparation used.

[$^3$H]Adenosine is transported from the circulating blood to the retina across the BRB with an apparent influx clearance of 11.1±4.1 μL/(min g retina) (Fig. 5). This value is far greater than that of [$^{14}$C]sucrose [0.26 μL/(min g retina)] and [$^3$H]D-mannitol [0.75 μL/(min g retina)] used as non-permeable paracellular markers [29]. The RUI value of [$^3$H]adenosine was also greater than that of [$^3$H]D-mannitol (Table 2). These results suggest that adenosine is transported via a carrier-mediated transport process, rather than by passive diffusion. Moreover, [$^3$H]adenosine uptake into the retina was inhibited by adenosine and thymidine, but was unaffected by cytidine (Table 2). These inhibitory characteristics are comparable with those obtained in TR-iBRB2 cells (Table 1). The BRB is composed of retinal capillary endothelial cells (inner BRB) and retinal pigment epithelial cells (outer BRB). In addition to TR-iBRB2 cells (Fig. 2), carrier-mediated adenosine transport has also been demonstrated in ARPE-19 cells, an in vitro model of the human outer BRB [30]. Accordingly, both the inner and outer BRB seem to be involved in [$^3$H]adenosine transport from the circulating blood to the retina. The net flux of adenosine transport at the BRB is still uncertain at the present time, since it is technically impossible to estimate the efflux clearance across the BRB. In the case of the blood–brain barrier (BBB), the efflux clearance of adenosine across the BBB is 3-fold greater than the influx clearance [31]. The adenosine concentration in the rat retina/choroid [32] (approximately 0.9 nmol/g ≈ 0.9 μM) is about 10-fold greater than that in the blood (90 nM) [31]. Since the $K_m$ of adenosine uptake by TR-iBRB2 cells (28.5 μM; Fig. 3) is greater than the adenosine concentration in the retina/choroid as well as the blood, the transport velocity of adenosine at the inner BRB is expected to be relative to the adenosine concentration. Therefore, the net efflux of adenosine transport at the inner BRB may occur as at the BBB [31], since ENT2 is a bi-directional equilibrative transporter.

In conclusion, adenosine transport at the inner BRB is most likely mediated by ENT2. Under physiological conditions, adenosine serves as the principal mechanism of inhibitory neuromodulation [33]. However, the adenosine concentration is dramatically increased by more than 10-fold in the ischemic retina [32] and then adenosine exacerbates the effects of retinal ischemia/reperfusion and promotes retinal neovascularization [2,34]. Therefore, the possible physiological role for ENT2 at the inner BRB involves maintaining a constant milieu of adenosine in the retinal interstitial fluid especially under some pathological conditions like ischemia. The current findings represent an important contribution to our understanding of the physiological roles of the inner BRB in regulating the adenosine concentration in the retina.

## Acknowledgements

The authors would like to thank Dr. Kazunori Katayama (University of Toyama) and Yoshiharu Deguchi (Teikyo University) for valuable discussions. This study was supported, in part, by a Grant-in-Aid for Scientific Research from the Japan Society for the Promotion of Science and a grant for Research on Sensory and Communicative Disorders by the Ministry of Health, Labor, and Welfare, Japan.

## References

[1] G.A. Lutty, D.S. McLeod, Retinal vascular development and oxygen-induced retinopathy: a role for adenosine, Prog. Retin. Eye Res. 22 (2003) 95–111.
[2] G.J. Ghiardi, J.M. Gidday, S. Roth, The purine nucleoside adenosine in retinal ischemia–reperfusion injury, Vis. Res. 39 (1999) 2519–2535.
[3] G.W. Kreutzberg, S.T. Hussain, Cytochemical heterogeneity of the glial plasma membrane: 5′-nucleotidase in retinal Müller cells, J. Neurocytol. 11 (1982) 53–64.
[4] G.A. Lutty, C. Merges, D.S. McLeod, 5′ nucleotidase and adenosine during retinal vasculogenesis and oxygen-induced retinopathy, Investig. Ophthalmol. Vis. Sci. 41 (2000) 218–229.
[5] L. Sosula, P. Beaumont, K.M. Jonson, F.C. Hollows, Quantitative ultrastructure of capillaries in the rat retina, Invest. Ophthalmol. 11 (1972) 916–925.
[6] K. Hosoya, M. Tomi, Advances in the cell biology of transport via the inner blood–retinal barrier: establishment of cell lines and transport functions, Biol. Pharm. Bull. 28 (2005) 1–8.
[7] E. Polska, P. Ehrlich, A. Luksch, G. Fuchsjager-Mayrl, L. Schmetterer, Effects of adenosine on intraocular pressure, optic nerve head blood flow, and choroidal blood flow in healthy humans, Investig. Ophthalmol. Vis. Sci. 44 (2003) 3110–3114.
[8] S.A. Baldwin, P.R. Beal, S.Y. Yao, A.E. King, C.E. Cass, J.D. Young, The equilibrative nucleoside transporter family, SLC29, Pflugers Arch. 447 (2004) 735–743.
[9] J.H. Gray, R.P. Owen, K.M. Giacomini, The concentrative nucleoside transporter family, SLC28, Pflugers Arch. 447 (2004) 728–734.
[10] M.A. Ackley, R.J. Governo, C.E. Cass, J.D. Young, S.A. Baldwin, A.E. King, Control of glutamatergic neurotransmission in the rat spinal dorsal horn by the nucleoside transporter ENT1, J. Physiol. 548 (2003) 507–517.
[11] B.J. Meester, N.P. Shankley, N.J. Welsh, F.L. Meijler, J.W. Black, Pharmacological analysis of the activity of the adenosine uptake inhibitor, dipyridamole, on the sinoatrial and atrioventricular nodes of the guinea-pig, Br. J. Pharmacol. 124 (1998) 729–741.
[12] C. Blazynski, The accumulation of [$^3$H]phenylisopropyl adenosine ([3H] PIA) and [$^3$H]adenosine into rabbit retinal neurons is inhibited by nitrobenzylthioinosine (NBI), Neurosci. Lett. 121 (1991) 1–4.
[13] R. Paes de Carvalho, K.M. Braas, S.H. Snyder, R. Adler, Analysis of adenosine immunoreactivity, uptake, and release in purified cultures of developing chick embryo retinal neurons and photoreceptors, J. Neurochem. 55 (1990) 1603–1611.
[14] K. Hosoya, M. Tomi, S. Ohtsuki, H. Takanaga, M. Ueda, N. Yanai, M. Obinata, T. Terasaki, Conditionally immortalized retinal capillary endothelial cell lines (TR-iBRB) expressing differentiated endothelial cell functions derived from a transgenic rat, Exp. Eye Res. 72 (2001) 163–172.
[15] K. Hosoya, A. Minamizono, K. Katayama, T. Terasaki, M. Tomi, Vitamin C transport in oxidized form across the rat blood–retinal barrier, Investig. Ophthalmol. Vis. Sci. 45 (2004) 1232–1239.
[16] T. Nakashima, M. Tomi, K. Katayama, M. Tachikawa, M. Watanabe, T. Terasaki, K. Hosoya, Blood-to-retina transport of creatine via creatine transporter (CRT) at the rat inner blood–retinal barrier, J. Neurochem. 89 (2004) 1454–1461.
[17] M. Tomi, M. Mori, M. Tachikawa, K. Katayama, T. Terasaki, K. Hosoya, L-Type amino acid transporter 1 (LAT1)-mediated L-leucine transport at

the inner blood–retinal barrier, Investig. Ophthalmol. Vis. Sci. 46 (2005) 2522–2530.
[18] T. Kitano, H. Iizasa, T. Terasaki, T. Asashima, N. Matsunaga, N. Utoguchi, Y. Watanabe, M. Obinata, M. Ueda, E. Nakashima, Polarized glucose transporters and mRNA expression properties in newly developed rat syncytiotrophoblast cell lines, TR-TBTs, J. Cell. Physiol. 193 (2002) 208–218.
[19] K. Yamaoka, Y. Tanigawara, T. Nakagawa, T. Uno, A pharmacokinetic analysis program (multi) for microcomputer, J. Pharmacobio-dyn. 4 (1981) 879–885.
[20] Y.S. Kang, T. Terasaki, A. Tsuji, Acidic drug transport in vivo through the blood–brain barrier. A role of the transport carrier for monocarboxylic acids, J. Pharmacobio-dyn. 13 (1990) 158–163.
[21] A. Alm, P. Törnquist, The uptake index method applied to studies on the blood–retinal barrier. I. A methodological study, Acta Physiol. Scand. 113 (1981) 73–79.
[22] E. Snoeck, K. Ver Donck, P. Jacqmin, H. Van Belle, A.G. Dupont, A. Van Peer, M. Danhof, Physiological red blood cell kinetic model to explain the apparent discrepancy between adenosine breakdown inhibition and nucleoside transporter occupancy of draflazine, J. Pharmacol. Exp. Ther. 286 (1998) 142–149.
[23] S.Y. Yao, A.M. Ng, W.R. Muzyka, M. Griffiths, C.E. Cass, S.A. Baldwin, J.D. Young, Molecular cloning and functional characterization of nitrobenzylthioinosine (NBMPR)-sensitive (es) and NBMPR-insensitive (ei) equilibrative nucleoside transporter proteins (rENT1 and rENT2) from rat tissues, J. Biol. Chem. 272 (1997) 28423–28430.
[24] J.L. Ward, A. Sherali, Z.P. Mo, C.M. Tse, Kinetic and pharmacological properties of cloned human equilibrative nucleoside transporters, ENT1 and ENT2, stably expressed in nucleoside transporter-deficient PK15 cells. ENT2 exhibits a low affinity for guanosine and cytidine but a high affinity for inosine, J. Biol. Chem. 275 (2000) 8375–8381.
[25] S.Y. Yao, A.M. Ng, M.F. Vickers, M. Sundaram, C.E. Cass, S.A. Baldwin, J.D. Young, Functional and molecular characterization of nucleobase transport by recombinant human and rat equilibrative nucleoside transporters 1 and 2. Chimeric constructs reveal a role for the ENT2 helix 5–6 region in nucleobase translocation, J. Biol. Chem. 277 (2002) 24938–24948.
[26] C.J. Sinclair, C.G. LaRiviere, J.D. Young, C.E. Cass, S.A. Baldwin, F. E. Parkinson, Purine uptake and release in rat C6 glioma cells: nucleoside transport and purine metabolism under ATP-depleting conditions, J. Neurochem. 75 (2000) 1528–1538.
[27] M. Chishty, D.J. Begley, N.J. Abbott, A. Reichel, Functional characterisation of nucleoside transport in rat brain endothelial cells, NeuroReport 14 (2003) 1087–1090.
[28] F.E. Parkinson, J. Friesen, L. Krizanac-Bengez, D. Janigro, Use of a three-dimensional in vitro model of the rat blood–brain barrier to assay nucleoside efflux from brain, Brain Res. 980 (2003) 233–241.
[29] S.L. Lightman, A.G. Palestine, S.I. Rapoport, E. Rechthand, Quantitative assessment of the permeability of the rat blood–retinal barrier to small water-soluble non-electrolytes, J. Physiol. 389 (1987) 483–490.
[30] S. Majumdar, S. Macha, D. Pal, A.K. Mitra, Mechanism of ganciclovir uptake by rabbit retina and human retinal pigmented epithelium cell line ARPE-19, Curr. Eye Res. 29 (2004) 127–136.
[31] A.J. Isakovic, N.J. Abbott, Z.B. Redzic, Brain to blood efflux transport of adenosine: blood–brain barrier studies in the rat, J. Neurochem. 90 (2004) 272–286.
[32] S. Roth, P.S. Rosenbaum, J. Osinski, S.S. Park, A.Y. Toledano, B. Li, A.A. Moshfeghi, Ischemia induces significant changes in purine nucleoside concentration in the retina-choroid in rats, Exp. Eye Res. 65 (1997) 771–779.
[33] E.A. Newman, Glial cell inhibition of neurons by release of ATP, J. Neurosci. 23 (2003) 1659–1666.
[34] R.P. Mino, P.E. Spoerri, S. Caballero, D. Player, L. Belardinelli, I. Biaggioni, M.B. Grant, Adenosine receptor antagonists and retinal neovascularization in vivo, Investig. Ophthalmol. Vis. Sci. 42 (2001) 3320–3324.

ELSEVIER

Journal of Neuroscience Methods 156 (2006) 249–256

JOURNAL OF NEUROSCIENCE METHODS

www.elsevier.com/locate/jneumeth

# Application of microdialysis to evaluate the efflux transport of estradiol 17-β glucuronide across the rat blood–retinal barrier

Kazunori Katayama, Yuki Ohshima, Masatoshi Tomi, Ken-ichi Hosoya*

*Department of Pharmaceutics, Graduate School of Medical and Pharmaceutical Sciences, University of Toyama, 2630 Sugitani, Toyama 930-0194, Japan*

Received 9 February 2006; received in revised form 9 March 2006; accepted 14 March 2006

**Abstract**

The purpose of the present study was to evaluate vitreous humor/retina-to-blood efflux transport in rats and determine the efflux transport of estradiol 17-β glucuronide (E17βG) across the blood–retinal barrier (BRB) by the use of microdialysis. [$^3$H]E17βG and [$^{14}$C]D-mannitol, which were used as a model compound for amphipathic organic anions and a bulk flow marker, respectively, were injected into the vitreous humor of rat eye, and a microdialysis probe was placed in the vitreous humor. [$^3$H]E17βG and [$^{14}$C]D-mannitol were bi-exponentially eliminated from the vitreous humor after vitreous bolus injection. The elimination rate constant of [$^3$H]E17βG during the terminal phase was 1.9-fold greater than that of [$^{14}$C]D-mannitol and reduced the level of [$^{14}$C]D-mannitol in the retinal presence of 0.3 mM E17βG, suggesting that [$^3$H]E17βG is transported via a carrier-mediated efflux transport process across the BRB. The efflux transport of [$^3$H]E17βG was significantly inhibited by organic anions, such as probenecid, sulfobromophthalein, digoxin, and dehydroepiandrosterone sulfate, whereas it was not inhibited by *p*-aminohippuric acid. In conclusion, the efflux transport of [$^3$H]E17βG across the rat BRB was evaluated by microdialysis and its inhibition by organic anions suggests organic anion transporting polypeptide 1a4-mediated E17βG efflux transport at the BRB.


*Keywords:* Blood–retinal barrier; Microdialysis; Organic anion; Organic anion transporting polypeptide (Oatp)1a4; Efflux transport

## 1. Introduction

The blood–retinal barrier (BRB), which forms complex tight junctions of retinal capillary endothelial cells (inner BRB) and retinal pigment epithelial cells (RPE; outer BRB), maintains a constant milieu and shields the neural retina from the circulating blood (Cunha-Vaz, 2004; Hosoya and Tomi, 2005). In addition to the structural barrier, the inner BRB expresses P-glycoprotein, which appears to restrict the blood-to-retina transport of hydrophobic drugs, such as cyclosporin A and quinidine (BenEzra and Maftzir, 1990; Duvvuri et al., 2003; Hosoya and Tomi, 2005). It is important to characterize influx and efflux transport processes at the BRB for drug distribution to the retina since the pharmacological effects of the drug in that tissue are governed by the retinal drug concentration. The blood-to-retina influx transport of the substrates has been investigated using the retinal uptake index method (Alm and Törnquist, 1981) and in vivo integration plot analysis (Hosoya et al., 2004), but it is limited to an evaluation of the retina-to-blood efflux transport of the substrates. It is important to elucidate the retina-to-blood efflux transport processes for organic anions since drugs, hormones, and neurotransmitters are mostly metabolized in the form of organic anions in the retina and need to undergo efflux transport from the retina to the blood across the BRB.

Vitreous fluorophotometry has been used to determine the transport of fluorescein, an organic anion, across the BRB in the blood-to-vitreous humor direction as well as in the opposite direction (Cunha-Vaz and Maurice, 1969; Engler et al., 1994). Engler et al. (1994) found that the fluorescein transport in the vitreous humor-to-blood direction is more than 100-fold greater than that in the opposite direction and is inhibited in the presence of probenecid, suggesting that fluorescein transported across the BRB is involved in the carrier-mediated organic anion transport process. Although this method is very useful for monitoring the integrity of the BRB, it is of limited value for studying the efflux transport of other organic anions since it is necessary to use a fluorescent probe.

Microdialysis has been recognized as a valuable tool for sampling the extracellular space of living tissue (Deguchi and Morimoto, 2001; Tunblad et al., 2004). This has been applied to

* Corresponding author. Tel.: +81 76 434 7505; fax: +81 76 434 5172.
*E-mail address:* hosoyak@pha.u-toyama.ac.jp (K.-i. Hosoya).

0165-0270/$ – see front matter © 2006 Elsevier B.V. All rights reserved.
doi:10.1016/j.jneumeth.2006.03.012

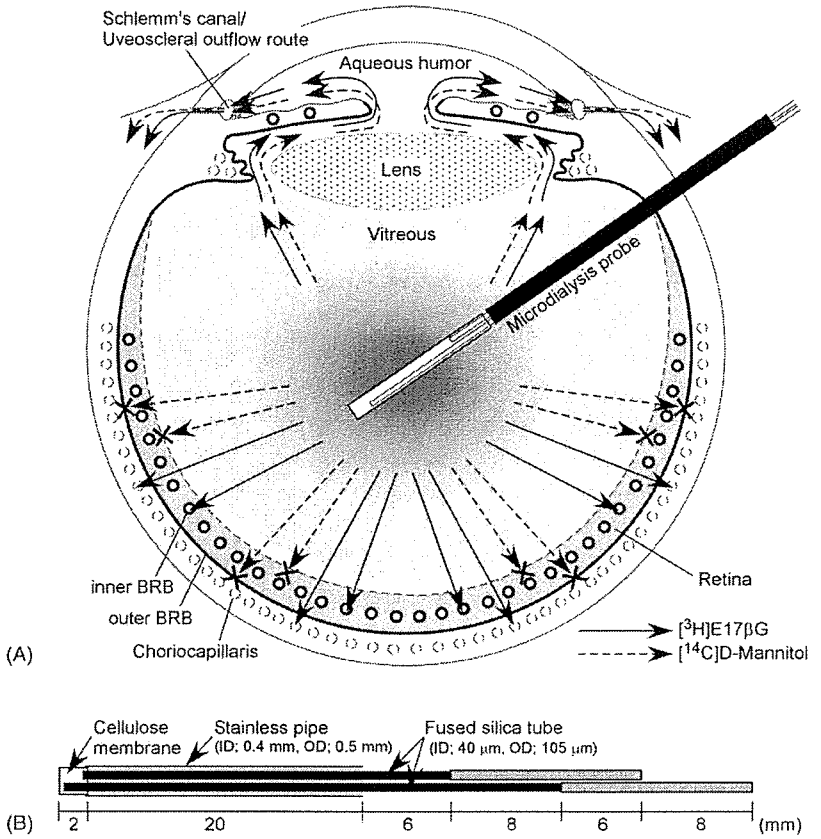


Fig. 1. Diagrammatic representation of the routes of elimination of [$^3$H]E17βG and [$^{14}$C]D-mannitol after vitreous bolus injection (A) and microdialysis probe (B). The microdialysis probe is implanted after vitreous bolus injection of both [$^3$H]E17βG and [$^{14}$C]D-mannitol. Bold and dashed lines represent the tight epithelial barrier and porous tissue boundary, respectively. Bold and dashed circles represent tight and fenestrated blood vessels, respectively (A). The custom-designed microdialysis probe (TEP-50) was constructed by Eicom (Kyoto, Japan) (B).

sampling vitreous fluid in the rabbit and monitoring drug concentrations in the vitreous humor (Anand et al., 2004; Macha and Mitra, 2001) and neurotransmitter concentrations in vitreous/retina tissue (Louzada-Junior et al., 1992). Macha and Mitra (2001) have reported the intravitreal kinetics of fluorescein after intravitreal administration using two microdialysis probes implanted in the anterior and vitreous chambers of the rabbit eye. The vitreous concentration of fluorescein decayed bi-exponentially and fluorescein appeared in the aqueous humor, suggesting that fluorescein is eliminated from the anterior chamber via Schlemm's canal and/or the uveoscleral outflow route as well as via the BRB (Engler et al., 1994; Macha and Mitra, 2001; Sears, 1983) (Fig. 1A). Although rabbits are generally used to evaluate the ocular kinetics of drugs because they have a similar size of eye compared with humans (Macha and Mitra, 2001; Rittenhouse et al., 1999), the anatomy of the rabbit eye is unusual among mammals. The retinal vessels are limited to a stripe of myelinated tissue that radiates horizontally from the optic nerve head, while the remainder of the retina is avascular (Pow, 2001; Sen et al., 1992) and drug transport between retina and blood is mainly via the outer BRB. The retinas in humans and rats are well vascularized and have an inner BRB as well as an outer BRB (Pow, 2001). Therefore, it is important to evaluate the vitreous humor/retina-to-blood efflux transport of organic anions in rats. Moreover, data can be compared with previous blood-to-retinal influx transport data generated from in vivo and in vitro studies in rats (Alm and Törnquist, 1981; Hosoya et al., 2001, 2004; Lightman et al., 1987).

The purpose of the present study was to carry out an in vivo evaluation of vitreous humor/retina-to-blood efflux transport in rats and determine the efflux transport of estradiol 17-β glucuronide (E17βG) across the BRB. We used a microdialysis probe, which was designed for the rat eye, and inserted it into the rat vitreous humor. Using this approach, we estimated the efflux transport of E17βG from the vitreous humor/retina to the blood across the BRB by monitoring the concentration of [$^3$H]E17βG and [$^{14}$C]D-mannitol, used as a model compound for amphipathic organic anions and a bulk flow marker, respectively, in the vitreous humor (Fig. 1).

## 2. Materials and methods

### 2.1. Animals

Male Wistar rats, weighing 250–300 g, were purchased from SLC (Shizuoka, Japan). The investigations using rats described in this report conformed to the provisions of the Animal Care Committee, Toyama Medical and Pharmaceutical University

(currently University of Toyama) (#2004-47) and the ARVO Statement on the Use of Animals in Ophthalmic and Vision Research.

### 2.2. Reagents

[Estradiol-6, 7-$^3$H(N)]-estradiol 17β-D-glucuronide ([$^3$H]E17βG, 45 Ci/mmol) and D-[1-$^{14}$C]-mannitol ([$^{14}$C]D-mannitol, 51 mCi/mmol) were purchased from Perkin-Elmer Life Sciences (Boston, MA). All other chemicals were of reagent grade and available commercially.

### 2.3. Theory

The diffusion-flow model for drug transfer through a microdialysis probe from the vitreous chamber is illustrated in Fig. 2. The membrane portion of the device containing the unstirred water layer in the vitreous humor is regarded as a membrane of thickness $L_M$ in which diffusion occurs in the $x$-direction. Thus, the flow of a drug in the membrane is given as

$$\frac{\partial C_M(t,x,z)}{\partial t} = D\frac{\partial^2 C_M(t,x,z)}{\partial x^2} \quad (1)$$

The initial condition of the equation is written as

$$t = 0, \quad C_M(t,x,z) = 0 \quad (2)$$

And the boundary conditions are as follows:

$$\text{(i)}\, x = 0, \quad C_M(t,x,z) = \varepsilon C_V(t) \quad (3)$$

$$\text{(ii)}\, x = L_M, \quad C_M(t,x,z) = \varepsilon C_T(t,z) \quad (4)$$

However, movement of drug in the tube portion of the device occurs through convective flow in the $z$-direction and diffusion through the membrane wall and the mass transfer equation is given as

$$\frac{\partial C_T(t,z)}{\partial t} = -v_Z\frac{\partial C_T(t,z)}{\partial z} - \frac{AD}{V}\left[\frac{\partial C_M(t,x,z)}{\partial x}\right]_{x=L_M} \quad (5)$$

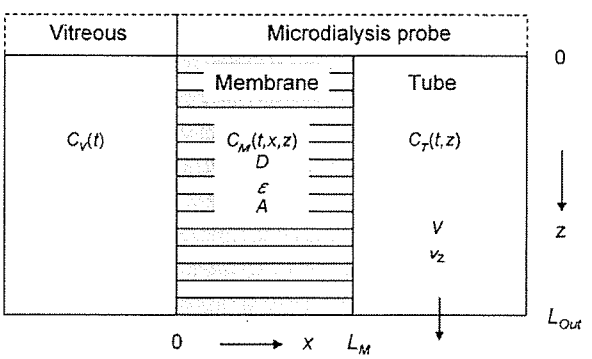


Fig. 2. Drug distribution between the microdialysis probe and the vitreous humor. $C_V$, concentration in the vitreous humor; $C_M$, concentration in the cellulose membrane; $C_T$, concentration in the tube; $D$, diffusion coefficient; $\varepsilon$, porosity; $A$, surface area; $V$, volume of the tube; $v_Z$, velocity of dialysate; $L_M$, membrane thickness; $x$, $x$-direction; $z$, $z$-direction; $L_{out}$, length between the tube inlet and outlet. $v_Z$ and $L_{out}$ were set at 6.37 cm/min and 2.0 mm, respectively.

The tube has an initial condition as follows:

$$t = 0, \quad C_T(t,z) = 0 \quad (6)$$

When the following variables are defined to simplify the solution, diffusion parameter: $D' = D/L_M^2$; partition parameter: $K' = \varepsilon L_M$; $d = \sqrt{s/D'}$; $\rho = A/V$, the Laplace transform of the outlet concentration of the microdialysis tube is given by (Appendix A)

$$\bar{C}_T(s, L_{out}) = \frac{\rho K'\bar{C}_V(s)}{\rho K'\cosh(d) + d\sinh(d)} \times \left\{1 - \exp\left[-s\left(1 + \frac{\rho K'}{d\tanh(d)}\right)\frac{L_{out}}{v_Z}\right]\right\} \quad (7)$$

#### 2.3.1. When the concentration of the vitreous humor is constant

If the drug concentration in the vitreous humor has a constant value, i.e., $C_V(t) = C_0$, Eq. (7) can be rewritten and drug concentration profile in the outlet is given by

$$\bar{C}_T(s, L_{out}) = \frac{\rho K' C_0}{s[\rho K'\cosh(d) + d\sinh(d)]} \times \left\{1 - \exp\left[-s\left(1 + \frac{\rho K'}{d\tanh(d)}\right)\frac{L_{out}}{v_Z}\right]\right\} \quad (8)$$

By using the final-value theorem, the outlet concentration in the tube under steady-state conditions is given as

$$\lim_{t\to\infty} C_T(t, L_{out}) = \lim_{s\to 0} s\bar{C}_T(s, L_{out}) = C_0\left[1 - \exp\left(-\rho K' D'\frac{L_{out}}{v_Z}\right)\right] \quad (9)$$

#### 2.3.2. When the concentration in the vitreous humor decays exponentially

If the drug concentration in the vitreous humor decreases in a mono-exponential fashion, i.e., $C_V(t) = C_0\exp(-\lambda_Z t)$, $C_T(t, L_{out})$ can be expressed by multi-exponential decay kinetics as follows (see Appendix B):

$$C_T(t, L_{out}) = U_Z\exp(-\lambda_Z t) + \sum_{n=1}^{n} U_n\exp(-D'\alpha_n^2 t) \quad (10)$$

where $U_Z$ and $U_n$ are given in Appendix B. Values for $\alpha_n$ are the roots of the following function:

$$\alpha_n\tan\alpha_n = \rho K' \quad (11)$$

Although Eq. (11) gives an infinite solution set, a single and minimum solution, $\alpha_1$ exists in the region $[0, \pi/2]$. According to Eq. (10), if $\lambda_Z$ is smaller than $D'\alpha_1^2$, the slope of drug concentration–time profiles in the outlet of the tube at a late time should be the same as that of the vitreous humor. However, if $\lambda_Z$ is larger than $D'\alpha_1^2$ in which membrane transport is rate-limiting, the proportional relationship between both concentrations will no longer hold.

### 2.4. Microdialysis study

The rats were anesthetized with an intraperitoneal injection of ketamine–xylazine (60 mg/kg ketamine and 15 mg/kg xylazine) and their heads were mounted on a stereotaxic frame (SR-6, Narishige, Tokyo, Japan). Their eyelids were locally anesthetized by instillation of 2% xylocaine and fixed using surgical sutures in order not to blink. A 25-gauge needle was inserted about 1 mm below the corneal scleral limbus through the pars plana at a depth of 3.0 mm. The needle was removed and [$^3$H]E17βG (5 μCi) and [$^{14}$C]D-mannitol (1 μCi) dissolved in 1.0 μL Ringer-HEPES solution (141 mM NaCl, 4.0 mM KCl, 2.8 mM $CaCl_2$, 10.0 mM HEPES, pH 7.4) was administered using a 10 μL microsyringe (Hamilton, Reno, NE) at a depth of 3.0 mm from the surface of the eye. The microdialysis probe was implanted immediately into the vitreous chamber and fixed with surgical glue (Aron Alpha A, Sankyo, Tokyo) on the surface of the eye. The custom-designed microdialysis probe (TEP-50, Fig. 1B) was constructed by Eicom (Kyoto, Japan). The length of the tubing (cellulose membrane) was 2.0 mm and the molecular cutoff for the dialysis tubing was 50 kDa. Ringer-HEPES solution at 37 °C was delivered to the probe continuously at 2 μL/min via polyethylene tubing (SP19, inner diameter 0.35 mm, outer diameter 1.05 mm, Natsume, Tokyo, Japan) connected to an infusion pump (model 11, Harvard, Holliston, MA). The dialysate was collected at 10 min intervals in vials over a period of 5 h, and the radioactivity in each fraction was determined by liquid scintillation counting.

For the experiment conducted in the presence of inhibitors, each inhibitor was dissolved in Ringer-HEPES solution and delivered to the probe as described above. The retinas were isolated at different time-intervals and the concentration of E17βG, probenecid, *p*-aminohippuric acid (PAH), sulfobromophthalein (BSP), and dehydroepiandrosterone sulfate (DHEAS) in the retina was determined by high-performance liquid chromatography (HPLC) using a 4.6 mm × 15 mm Inertsil ODS-2™ column (GL Sciences, Tokyo, Japan) and a UV monitor. The concentration of digoxin in the retina was determined using a kit (TDX™-digoxin, Abbott Japan, Tokyo, Japan). The plateau concentration of inhibitors in the retina was reached within 1 h.

The probe recovery was assessed in the in vitro medium containing a constant level of compounds and calculated as

$$\text{recovery}\,(\%) = \frac{C_T}{C_V} \times 100 \tag{12}$$

where $C_T$ (dpm/mL) is concentration of dialysate solution and $C_V$ (dpm/mL) is the concentration in the test solution or isolated vitreous humor. The vitreous humor was isolated and pre-equilibrated with test solution for 2 h. The parameters, $D'$ and $\rho K'$, were estimated using Eq. (8) with the non-linear least squares program MULTI (FILT) (Yano et al., 1989). We used a lag-time of 6 min for the passage through the polyethylene tubing connected to the distal end of the microdialysis probe. The recovery of [$^3$H]E17βG from the solution and vitreous humor was 3.51 ± 0.10% and 2.97 ± 0.09%, respectively. The recovery of [$^{14}$C]D-mannitol from the solution and vitreous humor was 3.96 ± 0.10% and 3.62 ± 0.16%, respectively. The recovery ratio from the solution and vitreous humor for [$^3$H]E17βG and [$^{14}$C]D-mannitol was 85% and 91%, respectively. The recovery of the probe in the vitreous chamber did not differ markedly from that in the test solution. The predicted values of $D'$ for [$^3$H]E17βG and [$^{14}$C]D-mannitol in the vitreous preparation (mean ± S.E.M., $n=3$) were 0.123 ± 0.007 and 0.127 ± 0.010 $\text{min}^{-1}$, respectively. The corresponding $\rho K'$ values for [$^3$H]E17βG and [$^{14}$C]D-mannitol were 7.72 ± 0.48 and 8.99 ± 0.74, respectively. Thus, the rate constant, $D'\alpha_1^2$ was expected to be within the range 0.3–0.4 $\text{min}^{-1}$ for both compounds. The value was much larger than that obtained for the in vivo terminal phase (see Section 3), suggesting that the transport across the microdialysis probe is not the rate-limiting step in vivo.

### 2.5. Determination of elimination profile after intravitreal injection

The vitreous concentrations normalized by the injected dose ($C_P$ (% dose/mL)), were estimated from the radioactivities in the dialysate using Eq. (13) and the $C_P$ at time $t$, $C_p(t)$ was fitted to a bi-exponential equation (Eq. (14)) by non-linear least squares regression analysis using the computer program MULTI (Yamaoka et al., 1981):

$$C_p = \frac{C_T}{\text{Dose}_{\text{tracer}}} \times 100 \tag{13}$$

$$C_p(t) = A\,e^{-\alpha t} + B\,e^{-\beta t} \tag{14}$$

where $C_T$ is the concentration in the dialysate (dpm/mL) and $\text{Dose}_{\text{tracer}}$ (dpm) is the total radioactivity of substance after intravitreal injection. The constants $A$ and $B$ are intercepts on the $y$-axis for each exponential segment of the curve in Eq. (14). The constants $\alpha$ and $\beta$ are the apparent first-order rate constants for the initial and terminal phase, respectively. The pharmacokinetic parameters ($A$, $\alpha$, $B$, and $\beta$) were successfully estimated by the damping Gauss–Newton method.

Unless otherwise indicated, all data represent means ± S.E.M. An unpaired, two-tailed Student's $t$-test was used to determine the significance of differences between two group means. Statistical significance of differences among means of several groups was determined by one-way analysis of variance (ANOVA) followed by the modified Fisher's least squares difference method.

## 3. Results

### 3.1. Elimination of [$^3$H]E17βG from the vitreous humor in vivo

Fig. 3A shows a typical elimination curve of [$^3$H]E17βG and [$^{14}$C]D-mannitol from the vitreous humor after bolus injection. [$^3$H]E17βG and [$^{14}$C]D-mannitol were bi-exponentially eliminated from the vitreous humor. Although the first rapid decline was almost the same for both compounds, the second decline in [$^3$H]E17βG was significantly greater than that of [$^{14}$C]D-mannitol (Fig. 3A). The elimination rate constant ($\beta$) of [$^3$H]E17βG during the terminal phase was 9.32 ± 0.83 × $10^{-3}$ $\text{min}^{-1}$ ($n=5$), which was 1.9-fold greater

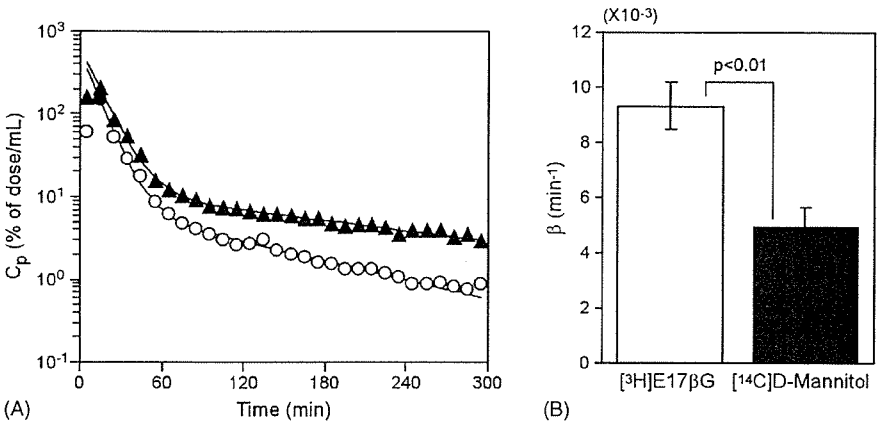


Fig. 3. Typical outflow pattern of [$^3$H]E17βG and [$^{14}$C]D-mannitol from the microdialysis probe (A) and elimination rate constants (β) of [$^3$H]E17βG and [$^{14}$C]D-mannitol during the terminal phase (B). Closed triangles and open circles represent the concentration in dialysate of [$^{14}$C]D-mannitol and [$^3$H]E17βG, respectively (A). Each column represents the mean ± S.E.M. ($n=5$) (B).

than that of [$^{14}$C]D-mannitol ($4.97 \pm 0.69 \times 10^{-3}$ min$^{-1}$, $n=5$) (Fig. 3B), supporting the hypothesis that elimination rate difference between [$^3$H]E17βG and [$^{14}$C]D-mannitol during the terminal phase involves efflux transport of [$^3$H]E17βG across the BRB.

### 3.2. Effect of several organic anions on the efflux transport of [$^3$H]E17βG

To examine whether the difference between the β-value of [$^3$H]E17βG and [$^{14}$C]D-mannitol contributes carrier-mediated efflux transport of E17βG, inhibition study was performed. The β-value of [$^3$H]E17βG was significantly reduced in the presence of 0.3 mM E17βG, 1.0 mM probenecid, 0.6 mM BSP, 0.1 mM DHEAS and 0.35 μM digoxin in the retina, whereas 0.7 mM PAH in the retina had no effect. On the other hand, the β-value of [$^{14}$C]D-mannitol was unchanged in the presence of all the inhibitors (Table 1), showing that inhibitors do not affect [$^{14}$C]D-mannitol transport. Fig. 4 shows the elimination rate differences between [$^3$H]E17βG and [$^{14}$C]D-mannitol during the terminal phase. In the presence of 0.3 mM E17βG in the retina, the efflux of [$^3$H]E17βG across the BRB was inhibited by 90.6%, suggesting that E17βG is transported via a carrier-mediated efflux transport process across the BRB. Moreover, 1.0 mM probenecid, and 0.6 mM BSP in the retina inhibited the efflux transport of [$^3$H]E17βG by 99.5% and 93.8%, respectively. DHEAS at 0.1 mM and digoxin at 0.35 μM in the retina reduced [$^3$H]E17βG efflux transport by 71.5% and 83.2%, respectively. In contrast, another organic anion, PAH at 0.7 mM, in the retina had no effect on [$^3$H]E17βG efflux transport.

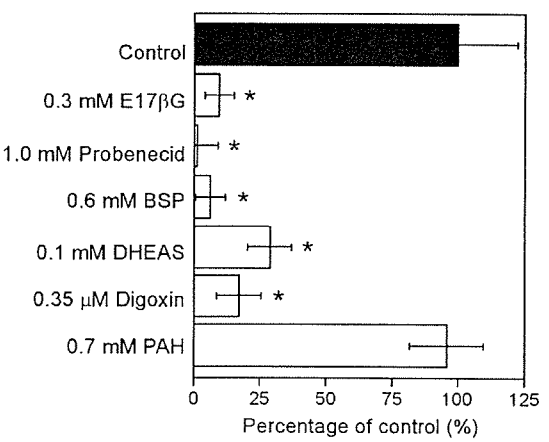


Fig. 4. Elimination rate difference between [$^3$H]E17βG and [$^{14}$C]D-mannitol during the terminal phase. Each column represents the mean ± S.E.M. ($n=4$–6). *$p<0.01$, significantly different from the control. Percentage of control was calculated from data in Table 1 as follows: {β-value of [$^3$H]E17βG − β-value of [$^{14}$C]D-mannitol in the presence of inhibitor}/{β-value of [$^3$H]E17βG − β-value of [$^{14}$C]D-mannitol in the absence of inhibitor} × 100.

Table 1
Effect of inhibitors on elimination rate constants (β) of [$^3$H]E17βG and [$^{14}$C]D-mannitol during the terminal phase

| Inhibitors (retinal concentration) | β (×10$^{-3}$ min$^{-1}$) | |
|---|---|---|
| | [$^3$H]E17βG | [$^{14}$C]D-Mannitol |
| Control | 9.32 ± 0.08 | 4.97 ± 0.69 |
| E17βG (0.3 mM) | 6.62 ± 1.09* | 6.21 ± 0.92 |
| Probenecid (1.0 mM) | 5.65 ± 0.64* | 5.63 ± 1.01 |
| BSP (0.6 mM) | 5.87 ± 0.42* | 5.60 ± 0.31 |
| DHEAS (0.1 mM) | 5.83 ± 0.36* | 4.59 ± 0.23 |
| Digoxin (0.35 μM) | 6.03 ± 0.46* | 5.30 ± 0.27 |
| PAH (0.7 mM) | 10.3 ± 0.91 | 6.14 ± 0.31 |

Each inhibitor was continuously perfused through the microdialysis probe which was implanted into the vitreous chamber. Concentration of inhibitors in the retina was determined by HPLC or a kit (digoxin). Each value represents the mean ± S.E.M. ($n=4$–6). E17βG, estradiol 17-β glucuronide; BSP, sulfobromophthalein; DHEAS, dehydroepiandrosterone sulfate; PAH, *p*-aminohippuric acid.

* $p<0.01$ significantly different from the control.

## 4. Discussion

The present study is the first time to demonstrate the efflux transport of E17βG across the rat BRB by the use of in vivo microdialysis. The dialysate concentration of [$^3$H]E17βG and [$^{14}$C]D-mannitol in the vitreous humor via the microdialysis probe decayed in a bi-exponential manner (Fig. 3A). The first

slope of the drug concentration–time profile was steeper than that of the second. This supports the hypothesis that the first and second declines reflect diffusion into the vitreous humor, including the microdialysis tube, after vitreous bolus injection and the elimination from the vitreous humor of both compounds, respectively. Therefore, Eq. (10) can be used to estimate the vitreous concentration of drug via the microdialysis probe and the $\beta$-value of [$^3$H]E17βG and [$^{14}$C]D-mannitol was estimated by non-linear least squares fitting of a bi-exponential equation (Eq. (14)) to the vitreous concentration values. The $\beta$-value of [$^3$H]E17βG was 1.9-fold greater than that of [$^{14}$C]D-mannitol, which is a bulk flow marker for passage from the vitreous humor to Schlemm's canal and/or the uveoscleral outflow route (Fig. 3B). This result supports the hypothesis that [$^3$H]E17βG undergoes efflux transport across the BRB in addition to elimination from the vitreous humor via bulk flow and passive diffusion (Fig. 1A). Macha and Mitra (2001) used two microdialysis probes implanted in the rabbit anterior and vitreous chambers to show that the vitreous concentration of fluorescein decayed bi-exponentially after bolus injection into the vitreous humor and fluorescein appeared in aqueous humor, showing that fluorescien is eliminated from the anterior chamber via Schlemm's canal and/or the uveoscleral outflow route as well as via the BRB. This was in good agreement with our results. Since we used [$^{14}$C]D-mannitol as a bulk flow marker, the vitreous humor/retina-to-blood efflux transport of E17βG can be used to estimate the difference in the elimination rate between [$^3$H]E17βG and [$^{14}$C]D-mannitol during the terminal phase even when there was a single microdialysis probe in the vitreous humor.

BRB damage due to the implantation of a microdialysis probe would affect the estimation of the BRB efflux transport, particularly in the case of small molecules. Using [$^{14}$C]D-mannitol, a very slow permeable marker of the BRB (Lightman et al., 1987), the $\beta$-value of [$^{14}$C]D-mannitol was almost constant even when inhibitors are present in the retina (Table 1). These results suggest that only limited physical damage to the BRB was caused by the implantation of a microdialysis probe in the vitreous chamber.

In order to discover whether an organic anion transport process is involved in the efflux transport of E17βG at the BRB, a microdialysis study was performed in the presence of several organic anions. In the presence of 0.3 mM E17βG in the retina, the $\beta$-value of [$^3$H]E17βG was significantly reduced by the level of [$^{14}$C]D-mannitol (Table 1), suggesting that E17βG is transported via a carrier-mediated efflux transport process across the BRB. [$^3$H]E17βG efflux transport from rat vitreous humor/retina was significantly inhibited by probenecid, BSP, and DHEAS, but not by PAH (Fig. 4). This inhibition pattern agrees well with that of the organic anion transporting polypeptide (Oatp) family rather than the organic anion transporter (OAT) family (Reichel et al., 1999; Sekine et al., 2000; Sugiyama et al., 2001). Although Oatp and OAT family are sensitive for probenecid, BSP, and DHEAS, Oatp is PAH-insensitive organic anion transporter (Reichel et al., 1999; Sekine et al., 2000; Sugiyama et al., 2001). Moreover, [$^3$H]E17βG efflux transport was significantly inhibited by digoxin at 0.35 μM (Fig. 4). Although digoxin is a specific substrate for Oatp1a4 (Slc21a5; Oatp2) and Oatp4c1 (Slco4c1; Oatp-H) with a Michaelis–Menten constant of 0.24 and 8.0 μM, respectively, Oatp1a4 has higher affinity of digoxin than that of Oatp4c1 (Hagenbuch and Meier, 2003; Mikkaichi et al., 2004; Noé et al., 1997). These findings suggest that Oatp1a4 is involved in vitreous humor/retina-to-blood efflux transport of E17βG at the BRB. Gao et al. (2002) provided morphological evidence using immunofluorescence confocal microscopy, showing that Oatp1a4 is localized on the apical side of rat RPE (outer BRB) and at the inner BRB. In the rat brain, Oatp1a4 is localized on both the luminal and abluminal sides of the blood–brain barrier (BBB) (Gao et al., 1999). Although localization of Oatp1a4 at the inner BRB has not yet been demonstrated, the localization of Oatp1a4 at the inner BRB may be similar to that of the BBB. Using a combination of a magnetic isolation method for rat retinal vascular endothelial cells and real-time quantitative PCR analysis, we found recently that Oatp1a4 and 1c1 (Slc21a14; Oatp14) mRNA are predominantly expressed at the inner BRB (Tomi and Hosoya, 2004). Oatp1c1 has been identified as a BBB-specific anion transporter which has E17βG as a substrate (Li et al., 2001; Sugiyama et al., 2003). However, Oatp1c1 does not have a high affinity for digoxin (50% inhibition concentration >0.5 mM) (Sugiyama et al., 2003). Taking these results into consideration, Oatp1a4 is at least partly involved in the uptake of E17βG from the retina in the vitreous humor/retina-to-blood efflux transport process. However, the transport system at the basolateral side of the RPE and the involvement of other organic anion transporters, such as multidrug resistance associated protein (MRP) and the OAT family, at the BRB are unclear and remain the subject of ongoing investigation.

In conclusion, the efflux transport of [$^3$H]E17βG across the rat BRB has been evaluated by application of a microdialysis probe to the vitreous humor. A functional in vivo inhibition study suggests that the BRB is involved in the efflux transport of E17βG, at least as far as Oatp1a4 is concerned. To the best of our knowledge, this is the first report to characterize the efflux transport of organic anions at the rat BRB in vivo. These findings provide important information about the physiological role of the BRB and how the BRB restricts amphipathic organic anions distribution to the retina.

## Acknowledgements

The authors would like to thank Dr. Junichi Kawakami for valuable discussions. This study was supported, in part, by a Grant-in-Aid for Scientific Research from the Japan Society for the Promotion of Science and a grant for Research on Sensory and Communicative Disorders by the Ministry of Health, Labor, and Welfare, Japan.

## Appendix A

We proposed the Laplace transforms $\bar{C}_V(s)$, $\bar{C}_M(s, x, z)$ and $\bar{C}_T(s, z)$ for the functions of time, $C_V(t)$, $C_M(t, x, z)$ and $C_T(t, z)$, respectively. The Laplace transformation of Eqs. (1) and (2)

is given as

$$s\bar{C}_M(s,x,z) = D\frac{\partial^2 \bar{C}_M(s,x,z)}{\partial x^2} \quad (A.1)$$

The general solution of Eq. (A.1) can be written as

$$\bar{C}_M(s,x,z) = A_1(z)\cosh\left(\sqrt{\frac{s}{D}}x\right) + A_2(z)\sinh\left(\sqrt{\frac{s}{D}}x\right) \quad (A.2)$$

The Laplace transforms corresponding to Eqs. (3) and (4) are:

$$\text{(i)}\ \bar{C}_M(s,0,z) = \varepsilon\bar{C}_V(s) \quad (A.3)$$

$$\text{(ii)}\ \bar{C}_M(s,L_M,z) = \varepsilon\bar{C}_T(s,z) \quad (A.4)$$

Substituting Eqs. (A.3) and (A.4) for (A.2) gives

$$A_1(z) = \varepsilon\bar{C}_V(s) \quad (A.5)$$

$$A_2(z) = \frac{\varepsilon}{\sinh(d)}[\bar{C}_T(s,z) - \bar{C}_V(s)\cosh(d)] \quad (A.6)$$

The equation corresponding to Eqs. (5) and (6) is

$$s\bar{C}_T(s,z) = -v_Z\frac{\partial\bar{C}_T(s,z)}{\partial z} - \rho D\left[\frac{\partial\bar{C}_M(s,x,z)}{\partial x}\right]_{x=L_M} \quad (A.7)$$

By rearranging Eq. (A.7), we obtain

$$v_Z\frac{\partial\bar{C}_T(s,z)}{\partial z} = -s\left[1+\frac{\rho K'}{d\tanh(d)}\right]\bar{C}_T(s,z) + s\frac{\rho K'}{d\sinh(d)}\bar{C}_V(s) \quad (A.8)$$

Integrating from $z=0$ to $L_{out}$, we get

$$\bar{C}_T(s,L_{out}) = \frac{f_1(s)\bar{C}_V(s)}{g_1(s)}\left[1-\exp\left(-\frac{sg_1(s)L_{out}}{v_Z}\right)\right] \quad (A.9)$$

where

$$f_1(s) = \frac{\rho K'}{d\sinh(d)} \quad (A.10)$$

$$g_1(s) = 1+\frac{\rho K'}{d\tanh(d)} \quad (A.11)$$

Eq. (A.9) is identical to Eq. (7) in the text.

## Appendix B

When the drug concentration in the vitreous humor decays exponentially, i.e., $C_V(t) = C_0\exp(-\lambda_Z t)$, $C_T(s,L_{out})$ is given as

$$\bar{C}_T(s,L_{out}) = \frac{f_2(s)}{g_2(s)} \quad (A.12)$$

where

$$f_2(s) = \rho K' C_0\left[1-\exp\left(-\frac{sg_1(s)L_{out}}{v_Z}\right)\right] \quad (A.13)$$

$$g_2(s) = (s+\lambda_Z)[d\sinh(d)+\rho K'\cosh(d)] \quad (A.14)$$

Eq. (A.12) can be split into partial fractions as

$$\bar{C}_T(s,L_{out}) = \frac{U_Z}{s+\lambda_Z} + \sum_{n=1}^{n}\frac{U_n}{s+D'\alpha_n^2} \quad (A.15)$$

where

$$U_Z = \left[\frac{f_2(s)}{g_2'(s)}\right]_{S=-\lambda_Z} = \frac{\rho K' C_0\left\{1-\exp\left[\left(1-\frac{\rho K'}{\sqrt{\frac{\lambda_Z}{D'}}\tan\sqrt{\frac{\lambda_Z}{D'}}}\right)\frac{\lambda_Z L_{out}}{v_Z}\right]\right\}}{-\sqrt{\frac{\lambda_Z}{D'}}\sin\sqrt{\frac{\lambda_Z}{D'}} + \rho K'\cos\sqrt{\frac{\lambda_Z}{D'}}} \quad (A.16)$$

$$U_n = \left[\frac{f_2(s)}{g_2'(s)}\right]_{S=-D'\alpha_n^2} = \frac{2\rho K' D'\alpha_n C_0\left\{1-\exp\left[\left(1-\frac{\rho K'}{\alpha_n\tan\alpha_n}\right)\frac{D'\alpha_n^2 L_{out}}{v_Z}\right]\right\}}{(D'\alpha_n^2-\lambda_Z)[(1+\rho K')\sin\alpha_n+\alpha_n\cos\alpha_n]} \quad (A.17)$$

The $\alpha_n$s are the roots of:

$$\alpha_n\tan\alpha_n = \rho K' \quad (A.18)$$

The inverse Laplace transform of Eq. (A.15) is reduced to Eq. (10) in the text.

## References


Alm A, Törnquist P. The uptake index method applied to studies on the blood–retinal barrier. Acta Physiol Scand 1981;113:73–9.

Anand BS, Atluri H, Mitra AK. Validation of an ocular microdialysis technique in rabbits with permanently implanted vitreous probes: systemic and intravitreal pharmacokinetics of fluorescein. Int J Pharm 2004;281:79–88.

BenEzra D, Maftzir G. Ocular penetration of cyclosporin A. The rabbit eye. Invest Ophthalmol Vis Sci 1990;31:1362–6.

Cunha-Vaz JG. The blood–retinal barriers system. Basic concepts and clinical evaluation. Exp Eye Res 2004;78:715–21.

Cunha-Vaz JG, Maurice D. Fluorescein dynamics in the eye. Doc Ophthalmol 1969;26:61–72.

Deguchi Y, Morimoto K. Application of an in vivo brain microdialysis technique to studies of drug transport across the blood–brain barrier. Curr Drug Metab 2001;2:411–23.

Duvvuri S, Gandhi MD, Mitra AK. Effect of P-glycoprotein on the ocular disposition of a model substrate, quinidine. Curr Eye Res 2003;27:345–53.

Engler CB, Sander B, Larsen M, Koefoed P, Parving HH, Lund-Andersen H. Probenecid inhibition of the outward transport of fluorescein across the human blood–retina barrier. Acta Ophthalmol 1994;72:663–7.

Gao B, Stieger B, Noé B, Fritschy JM, Meier PJ. Localization of the organic anion transporting polypeptide 2 (Oatp2) in capillary endothelium and choroid plexus epithelium of rat brain. J Histochem Cytochem 1999;47:1255–64.

Gao B, Wenzel A, Grimm C, Vavricka SR, Benke D, Meier PJ, et al. Localization of organic anion transport protein 2 in the apical region of rat retinal pigment epithelium. Invest Ophthalmol Vis Sci 2002;43:510–4.

Hagenbuch B, Meier PJ. The superfamily of organic anion transporting polypeptides. Biochim Biophys Acta 2003;1609:1–18.

Hosoya K, Tomi M. Advances in the cell biology of transport via the inner blood–retinal barrier: establishment of cell lines and transport functions. Biol Pharm Bull 2005;28:1–8.

Hosoya K, Tomi M, Ohtsuki S, Takanaga H, Ueda M, Yanai N, et al. Conditionally immortalized retinal capillary endothelial cell lines (TR-iBRB) expressing differentiated endothelial cell functions derived from a transgenic rat. Exp Eye Res 2001;72:163–72.

Hosoya K, Minamizono A, Katayama K, Terasaki T, Tomi M. Vitamin C transport in oxidized form across the rat blood–retinal barrier. Invest Ophthalmol Vis Sci 2004;45:1232–9.

Li JY, Boado RJ, Pardridge WM. Blood–brain barrier genomics. J Cereb Blood Flow Metab 2001;21:61–8.

Lightman SL, Palestine AG, Rapoport SI, Rechthand E. Quantitative assessment of the permeability of the rat blood–retinal barrier to small water-soluble non-electrolytes. J Physiol 1987;389:483–90.

Louzada-Junior P, Dias JJ, Santos WF, Lachat JJ, Bradford HF, Coutinho-Netto J. Glutamate release in experimental ischaemia of the retina: an approach using microdialysis. J Neurochem 1992;59:358–63.

Macha S, Mitra AK. Ocular pharmacokinetics in rabbits using a novel dual probe microdialysis technique. Exp Eye Res 2001;72:289–99.

Mikkaichi T, Suzuki T, Onogawa T, Tanemoto M, Mizutamari H, Okada M, et al. Isolation and characterization of a digoxin transporter and its rat homologue expressed in the kidney. Proc Natl Acad Sci USA 2004;101:3569–74.

Noé B, Hagenbuch B, Stieger B, Meier PJ. Isolation of a multispecific organic anion and cardiac glycoside transporter from rat brain. Proc Natl Acad Sci USA 1997;94:10346–50.

Pow DV. Amino acids and their transporters in the retina. Neurochem Int 2001;38:463–84.

Reichel C, Gao B, Van Montfoort J, Cattori V, Rahner C, Hagenbuch B, et al. Localization and function of the organic anion-transporting polypeptide Oatp2 in rat liver. Gastroenterology 1999;117:688–95.

Rittenhouse KD, Peiffer Jr RL, Pollack GM. Microdialysis evaluation of the ocular pharmacokinetics of propranolol in the conscious rabbit. Pharm Res 1999;16:736–42.

Sears ML. Pharmacology of the eye. New York: Springer-Verlag; 1983.

Sekine T, Cha SH, Endou H. The multispecific organic anion transporter (OAT) family. Pflügers Arch 2000;440:337–50.

Sen HA, Berkowitz BA, Ando N, de Juan Jr E. In vivo imaging of breakdown of the inner and outer blood–retinal barriers. Invest Ophthalmol Vis Sci 1992;33:3507–12.

Sugiyama D, Kusuhara H, Shitara Y, Abe T, Meier PJ, Sekine T, et al. Characterization of the efflux transport of 17beta-estradiol-D-17beta-glucuronide from the brain across the blood–brain barrier. J Pharmacol Exp Ther 2001;298:316–22.

Sugiyama D, Kusuhara H, Taniguchi H, Ishikawa S, Nozaki Y, Aburatani H, et al. Functional characterization of rat brain-specific organic anion transporter (Oatp14) at the blood–brain barrier: high affinity transporter for thyroxine. J Biol Chem 2003;278:43489–95.

Tomi M, Hosoya K. Application of magnetically isolated rat retinal vascular endothelial cells for the determination of transporter gene expression levels at the inner blood–retinal barrier. J Neurochem 2004;91:1244–8.

Tunblad K, Hammarlund-Udenaes M, Jonsson EN. An integrated model for the analysis of pharmacokinetic data from microdialysis experiments. Pharm Res 2004;21:1698–707.

Yamaoka K, Tanigawara Y, Nakagawa T, Uno T. A pharmacokinetic analysis program (multi) for microcomputer. J Pharmacobiodyn 1981;4:879–85.

Yano Y, Yamaoka K, Tanaka H. A nonlinear least squares program, MULTI (FILT), based on fast inverse Laplace transform for microcomputers. Chem Pharm Bull 1989;37:1035–8.

# Inhibition of Dehydroascorbic Acid Transport across the Rat Blood–Retinal and –Brain Barriers in Experimental Diabetes

Akito MINAMIZONO, Masatoshi TOMI, and Ken-ichi HOSOYA*

*Department of Pharmaceutics, Graduate School of Medical and Pharmaceutical Sciences, University of Toyama; 2630 Sugitani, Toyama 930–0194, Japan.* Received May 19, 2006; accepted July 20, 2006; published online July 25, 2006

**Vitamin C is mainly transported across the blood–retinal and –brain barriers as dehydroascorbic acid (DHA) *via* a facilitative glucose transporter, GLUT1, and accumulates as ascorbic acid in the retina and brain. To investigate whether DHA transport to the retina and brain is changed by hyperglycemia, [$^{14}$C]DHA transport across the blood–retinal and –brain barriers was examined using *in vivo* integration plot analysis in streptozotocin-induced diabetic rats with a 3-week duration of diabetes and in normal rats. Blood-to-retina and -brain transport of [$^{14}$C]DHA was reduced by 65.5% and 84.1%, respectively, in diabetic rats compared with normal rats, whereas there was no major difference in the heart. Therefore, we propose that hyperglycemia reduces the supply of vitamin C to the retina and brain.**

**Key words** dehydroascorbic acid; GLUT1; diabetes; blood–retinal barrier; blood–brain barrier

Vitamin C plays an essential role as a cofactor involved in the enzymatic biosynthesis of collagen, catecholamine, and peptide neurohormones and antioxidant and free radical scavengers to detoxify free radicals in the retina and brain.[1] Vitamin C is present in retinal and brain tissues at high concentrations compared with other organs and there is a greater than 10-fold gradient between the concentration of ascorbic acid (AA) in the retina and brain tissues and blood.[2,3] Recent reports indicate that vitamin C is mainly transported across the blood–retinal barrier (BRB) and –brain barrier (BBB) as dehydroascorbic acid (DHA) *via* a facilitative glucose transporter, GLUT1, and accumulates as AA in the retina and brain.[4—6] DHA, which is an oxidized form of AA, is present at a concentration of 10 $\mu$M in rat and human plasma.[7,8] To maintain a high concentration of AA in the retina and brain, GLUT1 at the BRB and BBB supplies DHA to the retina and brain as well as D-glucose under normal conditions. Thus, one hypothesis to explain its action in diabetes mellitus is that hyperglycemia inhibits the supply of DHA to the retina and brain because of competitive inhibition of D-glucose for DHA transport *via* GLUT1.

The purpose of this study was to evaluate how the DHA transport to the retina and brain changes under hyperglycemic conditions by using integration plot analysis in streptozotocin-induced diabetic and normal rats.

## MATERIALS AND METHODS

**Animals** Male Wistar rats at 3 weeks of age (body weights: 50—55 g) were purchased from SLC (Shizuoka, Japan). The investigations using rats described in this report conformed to the provisions of the Animal Care Committee, Toyama Medical and Pharmaceutical University (currently University of Toyama) (#2004-48) and the ARVO Statement on the Use of Animals in Ophthalmic and Vision Research.

**Regents** L-[1-$^{14}$C]Ascorbic acid ([$^{14}$C]AA, 13 mCi/mmol) was purchased from Perkin-Elmer Life Sciences (Boston, MA, U.S.A.). L-[$^{14}$C]Dehydroascorbic acid ([$^{14}$C]DHA) was generated in all experiments by incubating [$^{14}$C]AA (1 $\mu$M in saline) with ascorbate oxidase (1 unit/1 mmol AA in saline, Sigma, St. Louis, MO, U.S.A.) at 37 °C for 90 s as described in a previous report.[5] All other chemicals were of reagent grade and available commercially.

**Animal Model of Diabetes Melitus** Rats at 3 weeks of age were randomly assigned to become diabetic ($n$=5) or to remain non-diabetic controls ($n$=5). Diabetes was induced by the injection of a freshly prepared solution of streptozotocin in citrate buffer (pH 4.5) at a dose of 45 mg/kg into the tail vein, whereas non-diabetic control rats were treated with citrate buffer alone. A sample of blood was obtained from this vein over a period from 1 to 3 weeks after streptozotocin injection for measurement of the blood D-glucose concentrations to confirm the presence of hyperglycemia. Blood glucose concentrations were determined by the glucoseoxidase method (Nipro Freestyle, Osaka, Japan).

**Determination of Influx Permeability Clearance** The rats were anesthetized with an intramuscular injection of ketamine–xylazine (1.22 mg xylazine and 125 mg ketamine/kg) and then [$^{14}$C]DHA (5 $\mu$Ci/rat, approximately 200 $\mu$mol DHA in 200 $\mu$l/head) was injected *via* the femoral vein. At the times designated (0.5, 1, 3 or 5 min) after administration, rats were sacrificed and the plasma and tissues were removed. Tissue sampling and determination of radioactivity were performed as described in a previous report.[5] The apparent influx permeability clearance ($K_{in}$) of [$^{14}$C]DHA in the tissue ($K_{in\ tissue}$) [$\mu$l/(min·g tissue)] was determined by integration plot analysis. As an index of the tissue distribution characteristics of [$^{14}$C]DHA, the apparent tissue-to-plasma concentration ratio ($V_d$) was used. This ratio [$V_d(t)$] (ml/g tissue) was defined as the amount of [$^{14}$C] per gram tissue divided by that per milliliter plasma, calculated over the time-period of the experiment. In brief, the tissue uptake rate of [$^{14}$C]DHA can be described by equation (Eq. 1):

$$V_d(t)=K_{in}\times AUC(t)/C_p(t)+V_i \quad (1)$$

where $C_p(t)$ (dpm/ml) and $V_i$ (ml/g tissue) represent the plasma concentration at time $t$ and the rapidly equilibrated distribution volume of [$^{14}$C]DHA, respectively; $AUC(t)$ (dpm·min/ml) is the area under the plasma concentration time curve of [$^{14}$C]DHA from time 0 to $t$. When $AUC(t)/C_p(t)$ (min) is plotted *versus* $V_d(t)$ (ml/g tissue), as shown in Fig. 1, the slope represents $K_{in\ tissue}$ [$\mu$l/(min·g tissue)].

* To whom correspondence should be addressed. e-mail: hosoyak@pha.u-toyama.ac.jp

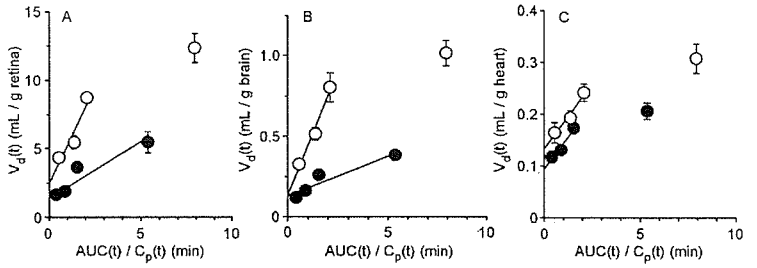


Fig. 1. Integration Plot of the Initial Uptake of [$^{14}$C]DHA by the Retina (A), Brain (B), and Heart (C) after Intravenous Administration

[$^{14}$C]DHA (5 $\mu$Ci/rat) was injected into streptozotocin-induced diabetic rats (closed circle) and normal rats (open circle) *via* the femoral vein. Each point represents the mean± S.E.M. ($n$=3—5).

**Data Analysis** Unless otherwise indicated, all data represent means±S.E.M. An unpaired, two-tailed Student's $t$-test was used to determine the significance of differences between two group means.

## RESULTS

The blood D-glucose concentration was 25.6±0.4 mM ($n$=5) in the streptozotocin-induced diabetic rats with a 3-week duration of diabetes, and 4.42±0.07 mM ($n$=10) and 8.01±0.32 mM ($n$=5) at 3 and 6 weeks age, respectively, in non-diabetic control rats. It was increased 3.2-fold in diabetic rats compared with controls. The final body weights were not appreciably increased in the streptozotocin-induced diabetic rats with a 3-week duration of diabetes (97.6±4.0 g, $n$=5), whereas the final body weights of the control rats increased to 215±5 g ($n$=5) from 52.0±1.0 g ($n$=10).

The DHA transport into the retina and brain across the BRB and BBB was evaluated and compared with the heart by means of the integration plot analysis after intravenous administration of [$^{14}$C]DHA to the streptozotocin-induced diabetic and normal rats (Fig. 1). The $K_{\text{in retina}}$ of [$^{14}$C]DHA in diabetic and normal rats was determined to be 841±243 $\mu$l/(min·g retina) and $2.44\times10^{3}\pm0.05\times10^{3}$ $\mu$l/(min·g retina), respectively. The $K_{\text{in brain}}$ of [$^{14}$C]DHA in diabetic and normal rats was determined to be 49.1± 11.5 $\mu$l/(min·g brain) and 309±53 $\mu$l/(min·g brain), respectively. The $K_{\text{in retina}}$ and $K_{\text{in brain}}$ of [$^{14}$C]DHA in diabetic rats was reduced by 65.5% and 84.1%, respectively, compared with normal rats, whereas no significant difference was found between the $K_{\text{in heart}}$ of diabetic and normal rats [50.0±12.6 $\mu$l/(min·g heart) and 49.7±15.1 $\mu$l/(min·g heart), respectively].

## DISCUSSION

The present study produces, for the first time, *in vivo* evidence that hyperglycemia reduces blood-to-retina and -brain transport of [$^{14}$C]DHA across the BRB and BBB (Fig. 1). DHA is transported by GLUT1, which is expressed at the luminal (blood) and abluminal (retina or brain) side of the inner BRB (retinal capillary endothelial cells), outer BRB (retinal pigment epithelial cells), and BBB (brain capillary endothelial cells).[9—11] On the other hand, there was only a small difference between the $K_{\text{in heart}}$ of diabetic and normal rats since there is no barrier in the heart. Therefore, DHA transport from blood to the retina and brain decreases with increasing blood D-glucose concentration because of prevention of DHA uptake by GLUT1 at the BRB and BBB. We previously reported that [$^{14}$C]DHA uptake by a retinal endothelial cell line (TR-iBRB2 cells) expressing GLUT1 was inhibited by D-glucose in a concentration-dependent manner with a 50% inhibition of 5.56 mM.[5] Although DHA transport *via* GLUT1 at the BRB and BBB is not completely inhibited under normal conditions, it is markedly inhibited under diabetic conditions. Indeed, the $K_{\text{in retina}}$ and $K_{\text{in brain}}$ of [$^{14}$C]DHA in diabetic rats was reduced by 65.5% and 84.1%, respectively, compared with normal rats (Fig. 1). Badr *et al.* reported that streptozotocin-induced diabetic rats with a 8-week duration of diabetes exhibited reduced GLUT1 expression by >60% at the inner BRB compared with non-diabetic rats, but this resulted in no reduction in GLUT1 expression at the outer BRB and BBB.[12] On the other hand, Pardridge *et al.* reported that streptozotocin-induced diabetic rats with a 1-week duration of diabetes exhibited reduced GLUT1 expression by 77% at the BBB compared with non-diabetic rats.[13] Although down-regulation of GLUT1 expression is not constant under different experimental conditions, reduction of GLUT1 expression at the BRB and BBB cannot be ruled out as a contributor to DHA transport to the retina and brain in the present study. When the GLUT1 expression at the BBB was reduced by 77%, the GLUT1 transport activity at the BBB was only reduced by 44%.[13] Therefore, hyperglycemia plays a role in reducing the supply of DHA to the brain and retina even although GLUT1 is down-regulated.

Since there is no compensatory down-regulation of GLUT1 at the inner BRB in an animal model and in patients with long-standing diabetes,[14,15] reduction of DHA transport by hyperglycemia is more involved in the chronic hyperglycemia of long-standing diabetes than acute hyperglycemia. The total vitamin C concentration in the retina and brain is not changed in short-term diabetics, since AA/DHA could be recycled by glutathione.[16,17] However, the chronic hyperglycemia of long-standing diabetes is associated with "glucose toxicity" leading to oxidative stress resulting from increased production of reactive oxygen species and, often, down-regulation of anti-oxidative defense mechanisms.[18,19] Hyperglycemia reduces DHA transport *via* GLUT1 at the BRB and BBB. DHA is reconverted into AA in the retina and brain.[4,5] Reduction of the supply of AA to the retina and brain through competition of D-glucose and DHA for a common transporter would reduce the antioxidant and could lead to accumulation of reactive oxygen species followed by acti-

vation of the protein kinase C and aldose reductase pathway and advanced glycation end-products in the retina and brain.[20] Moreover, AA is a required cofactor for several intracellular hydroxylases, including proline hydroxylase and dopamine-$\beta$-hydroxylase.[1] Therefore, chronic hyperglycemia appears to cause disregulation of catecholamine metabolism in the retina and brain. In the light of these findings, diabetic patients may experience enhanced oxidative stress and metabolic perturbations in the retina and brain by reducing the influx transport of DHA, leading to the hypothesis that diabetic retinopathy and encephalopathy involve a dysfunction of DHA influx transport at the BRB and BBB.

In conclusion, hyperglycemia reduces blood-to-retina and -brain transport of DHA across the BRB and BBB. These findings provide important information to help us understand the implications of increasing the antioxidant potential in the retina and brain.

**Acknowledgements** The authors would like to thank Drs. Kazunori Katayama and Ikuko Kimura for valuable discussions. This study was supported, in part, by a Grant-in-Aid for Scientific Research from the Japan Society for the Promotion of Science and a grant for Research on Sensory and Communicative Disorders by the Ministry of Health, Labor, and Welfare, Japan.

REFERENCES

1) Friedman P. A., Zeidel M. L., *Nature Med.*, **5**, 620—621 (1999).
2) Kaufman S., *Phamacol. Rev.*, **18**, 61—69 (1966).
3) Nielsen J. C., Naash M. I., Anderson R. E., *Invest. Ophthalmol. Vis. Sci.*, **29**, 22—26 (1987).
4) Agus D. B., Gambhir S. S., Pardridge W. M., Spielholz C., Baselga J., Vera J. C., Golde D. W., *J. Clin. Invest.*, **100**, 2842—2848 (1997).
5) Hosoya K., Minamizono A., Katayama K., Terasaki T., Tomi M., *Invest. Ophthalmol. Vis. Sci.*, **45**, 1232—1239 (2004).
6) Tomi M., Hosoya K., *J. Neurochem.*, **91**, 1244—1248 (2004).
7) Koshiishi I., Imanari T., *J. Chromatogr. B*, **709**, 150—156 (1998).
8) Nakayama H., Akiyama S., Inagaki M., Gotoh Y., Oguchi K., *Nephrol. Dial. Transplant.*, **16**, 574—579 (2001).
9) Pardridge W. M., Boado R. J., Farrell C. R., *J. Biol. Chem.*, **265**, 18035—18040 (1990).
10) Takata K., Kasahara T., Kasahara M., Ezaki O., Hirano H., *Invest. Ophthalmol. Vis. Sci.*, **33**, 377—383 (1992).
11) Kumagai A. K., Glasgow B. J., Pardridge W. M., *Invest. Ophthalmol. Vis. Sci.*, **35**, 2887—2894 (1994).
12) Badr G. A., Tang J., Ismail-Beigi F., Kern T. S., *Diabetes*, **49**, 1016—1021 (2000).
13) Pardridge W. M., Triguero D., Farrell C. R., *Diabetes*, **39**, 1040—1044 (1990).
14) Kumagai A. K., Vinorces S. A., Pardridge W. M., *Brain Res.*, **706**, 313—317 (1996).
15) Fernandes R., Suzuki K., Kumagai A. K., *Invest. Ophthalmol. Vis. Sci.*, **44**, 3150—3154 (2003).
16) May J. M., Qu Z., Li X., *Biochem. Pharmacol.*, **62**, 873—881 (2001).
17) Obrosova I. G., Minchenko A. G., Marinescu V., Fathallah L., Kennedy A., Stockert C. M., Frank R. N., Stevens M. J., *Diabetologia*, **44**, 1102—1110 (2001).
18) Lorenzi M., Gerhardinger C., *Diabetologia*, **44**, 791—804 (2001).
19) Mastrocola R., Restivo F., Vercellinatto I., Danni O., Brignardello E., Aragno M., Boccuzzi G., *J. Endocrinol.*, **187**, 37—44 (2005).
20) Root-Bernstein R., Busik J. V., Henry D. N., *J. Theor. Biol.*, **216**, 345—359 (2002).

0013-7227/06/$15.00/0
*Printed in U.S.A.*

Endocrinology 147(2):1020–1028

doi: 10.1210/en.2005-0825

# Altered Subcellular Distribution of Estrogen Receptor α Is Implicated in Estradiol-Induced Dual Regulation of Insulin Signaling in 3T3-L1 Adipocytes

Kiyofumi Nagira, Toshiyasu Sasaoka, Tsutomu Wada, Kazuhito Fukui, Mariko Ikubo, Satoko Hori, Hiroshi Tsuneki, Shigeru Saito, and Masashi Kobayashi

*Departments of Obstetrics and Gynecology (K.N., S.S.) and Clinical Pharmacology (T.W., S.H., H.T., T.S.) and First Department of Medicine (K.F., M.I., M.K.), University of Toyama, 2630 Sugitani, Toyama 930-0194, Japan*

**We investigated the mechanisms by which estrogen alters insulin signaling in 3T3-L1 adipocytes. Treatment with 17β-estradiol (E2) did not affect insulin-induced tyrosine phosphorylation of insulin receptor. E2 enhanced insulin-induced tyrosine phosphorylation of insulin receptor substrate-1 (IRS-1), IRS-1/p85 association, phosphorylation of Akt, and 2-deoxyglucose uptake at $10^{-8}$ M, but inhibited these effects at $10^{-5}$ M. A concentration of $10^{-5}$ M E2 enhanced insulin-induced phosphorylation of IRS-1 at $Ser^{307}$, which was abolished by treatment with a c-Jun $NH_2$-terminal kinase inhibitor. In addition, the effect of E2 was abrogated by pretreatment with a specific estrogen receptor antagonist, ICI182,780. Membrane-impermeable E2, E2-BSA, did not affect the insulin-induced phosphorylation of Akt at $10^{-8}$ M, but inhibited it at $10^{-5}$ M. Furthermore, E2 decreased the amount of estrogen receptor α at the plasma membrane at $10^{-8}$ M, but increased it at $10^{-5}$ M. In contrast, the subcellular distribution of estrogen receptor β was not altered by the treatment. These results indicate that E2 affects the metabolic action of insulin in a concentration-specific manner, that high concentrations of E2 inhibit insulin signaling by modulating phosphorylation of IRS-1 at $Ser^{307}$ via a c-Jun $NH_2$-terminal kinase-dependent pathway, and that the subcellular redistribution of estrogen receptor α in response to E2 may explain the dual effect of E2. (*Endocrinology* 147: 1020–1028, 2006)**

HUMAN PREGNANCY IS associated with hyperinsulinemia and a progressive decline in insulin sensitivity (1). Thus, a number of clinical studies indicate that insulin resistance occurs in late pregnancy (2, 3). The cellular changes in insulin resistance during late pregnancy have been ascribed to altered levels of placental-derived hormones, including estrogen, progesterone, and human placental lactogen (4). Among these sex steroids, high concentrations of estrogen are known to inhibit insulin-stimulated glucose uptake in cultured cells (5). In addition, increased levels of TNF-α have been associated with insulin resistance in late pregnancy (6). Thus, estrogen and TNF-α produced in the placenta appear to play a key role in insulin resistance (5, 6). Although the mechanism of insulin resistance caused by TNF-α has been studied intensively, the mechanism by which estrogen induces insulin resistance is unknown (6). In contrast, physiological levels of estrogen are known to protect against insulin resistance in women (7). Along this line, clinical studies suggest that after menopause women have an increased risk of developing diabetes (8, 9). Therefore, estrogen appears to control glucose homeostasis in a concentration-specific manner. The insulin signaling system leading to glucose uptake has been studied intensively in 3T3-L1 adipocytes (10).

The binding of insulin to the α-subunit of the insulin receptor results in autophosphorylation and activation of the β-subunit (11–13). The activated insulin receptor phosphorylates insulin receptor substrate-1 (IRS-1) at tyrosine residues (11–13). Tyrosine-phosphorylated IRS-1 binds to the p85 subunit of phosphatidylinositol 3-kinase (PI3-kinase), leading to the activation of the p110 catalytic subunit (11–13). PI3-kinase generates PI triphosphate from PI-bisphosphate, leading to the phosphorylation and activation of Akt (11–13). Akt is known to be an important mediator of the insulin-induced uptake of glucose (14). The cellular mechanisms by which estrogen affects the insulin signaling system are unknown.

Estrogen binds receptors of two subtypes: estrogen receptor α, first identified in 1986, and estrogen receptor β, cloned subsequently (15, 16). Estrogen receptors are expressed not only in the reproductive organs of males and females, but also in nonreproductive tissues, including fat tissues (17, 18). It has been shown that the effect of estrogen is mediated by the binding of estrogen receptors in the cytosol, resulting in translocation and transcriptional activation in the nucleus (19). In addition, recent reports suggest a nontranscriptional action mediated by the estrogen receptor (20). Along these lines, estrogen receptors are distributed in the plasma membrane in addition to the cytosol and nucleus (21). However, the role of estrogen receptors at specific cellular locations in the regulation of insulin signaling is unknown.

In the present study we studied the effect of the main estrogen, estradiol (E2), on insulin signaling leading to glucose uptake in 3T3-L1 adipocytes. In addition, to clarify the

First Published Online November 3, 2005

Abbreviations: 2-DOG, 2-Deoxyglucose; CS-, charcoal-stripped; E2, 17β-estradiol, estradiol; FBS, fetal bovine serum; HES, HEPES sucrose; IRS-1, insulin receptor substrate-1; JNK, c-Jun $NH_2$-terminal kinase; PI, phosphatidylinositol 3-kinase; PMSF, phenylmethylsulfonylfluoride.

*Endocrinology* is published monthly by The Endocrine Society (http://www.endo-society.org), the foremost professional society serving the endocrine community.

molecular mechanism by which E2 affects the insulin signaling system, we investigated the isoform and subcellular distribution of the estrogen receptor mediating the effect of E2.

## Materials and Methods

### *Materials*

Recombinant human insulin was provided by Lilly Research Laboratories (Indianapolis, IN). Recombinant human TNF-$\alpha$ was supplied by Dainippon Pharmaceutical Co. (Osaka, Japan). 17$\beta$-Estradiol (E2) and E2-BSA were purchased from Sigma-Aldrich Corp. (St. Louis, MO). A complete estrogen receptor antagonist, ICI182,780, was obtained from Tocris (Ellisville, MO). The Jun $NH_2$-terminal kinase (JNK) inhibitor, SP600125, was purchased from BIOMOL (Plymouth Meeting, PA). 2-[1,2-$^3$H]Deoxyglucose (2-DOG) was obtained from DuPont NEN Life Science Products (Boston, MA). A monoclonal antiphosphotyrosine antibody (PY20) was purchased from Transduction Laboratories (Lexington, KY). A polyclonal anti-IRS-1 antibody, a polyclonal anti-Ser$^{307}$ phosphospecific IRS-1 antibody, a polyclonal anti-Ser$^{612}$ phosphospecific IRS-1 antibody, a polyclonal anti-Ser$^{636}$ phosphospecific IRS-1 antibody, a monoclonal anti-p85 antibody, a polyclonal anti-Ser$^{473}$ phosphospecific Akt antibody, a polyclonal anti-Thr$^{308}$ phosphospecific Akt antibody, and a polyclonal anti-Akt antibody were obtained from Upstate Biotechnology, Inc. (Lake Placid, NY). A polyclonal antiinsulin receptor antibody, horseradish peroxidase-conjugated antimouse and antirabbit IgG antibodies, a polyclonal antiestrogen receptor $\alpha$ antibody, and a polyclonal antiestrogen receptor $\beta$ antibody were purchased from Santa Cruz Biotechnology, Inc. (Santa Cruz, CA). Phenol red-free DMEM and fetal bovine serum (FBS) were obtained from Invitrogen Life Technologies, Inc. (Gaithersburg, MD). Protein G-Sepharose was purchased from Pharmacia Biotech (Uppsala, Sweden). Reagents for electrophoresis were obtained from Bio-Rad Laboratories, Inc. (Hercules, CA). All other reagents were of analytical grade and purchased from Sigma-Aldrich Corp. or Wako Pure Chemical Industries (Osaka, Japan).

### *Cell culture and treatment*

3T3-L1 fibroblasts were grown and passaged in phenol red-free DMEM supplemented with 10% donor calf serum. Cells, 2 d after confluence, were used for differentiation. The differentiation medium contained 10% charcoal-stripped FBS (CS-FBS), 0.5 mM 3-isobutyl-1-methylxanthine, 1 $\mu$M dexamethasone, and 1 $\mu$M insulin. After charcoal stripping, E2 and estrone concentrations in serum decreased from 0.48 to less than 0.07 pM and from 0.36 to less than 0.12 pM, respectively. After 3 d, the differentiation medium was replaced with postdifferentiation medium containing 10% CS-FBS and 800 nM insulin. After 3 more days, the postdifferentiation medium was replaced with phenol red-free DMEM supplemented with 10% CS-FBS. The medium was changed every 3 d until the cells were used for experiments. Fourteen to 16 d after the induction of differentiation, more than 95% of the cells had morphological and biochemical properties of adipocytes. E2 dissolved in ethanol and TNF-$\alpha$ in PBS were added to the cell culture medium, in which $10^6$ cells were contained/plate, without FBS for 16 h.

### *2-DOG uptake*

3T3-L1 adipocytes derived from differentiation of 3T3-L1 fibroblasts were grown in six-well multiplates and were serum-starved for 3 h. The cells were stimulated with 17 nM insulin for 15 min in Krebs-Ringer-phosphate-HEPES buffer containing 10 mM HEPES, 131.2 mM NaCl, 4.7 mM KCl, 1.2 mM $MgSO_4$, 2.5 mM $CaCl_2$, and 2.5 mM $NaH_2PO_4$, and 1% BSA (pH 7.4). 2-[$^3$H]DOG (0.1 mM; 0.4 kBq/well) was added for 4 min. The reaction was stopped by the addition of 10 $\mu$M cytochalasin B. The cells were washed three times with ice-cold PBS and solubilized with 0.2% sodium dodecyl sulfate-0.2 N NaOH (22, 23). The radioactivity incorporated into the cells was measured by liquid scintillation counting. The results were corrected for nonspecific uptake determined by 2-[$^3$H]DOG uptake in the presence of 10 $\mu$M cytochalasin B. Nonspecific binding was less than 10% of the total uptake.

### *Subcellular fractionation*

The cells were washed twice with PBS and once with HEPES sucrose (HES) buffer containing 255 mM sucrose, 20 mM HEPES, 1 mM EDTA, 1 mM phenylmethylsulfonylfluoride (PMSF), 1 mM $Na_3VO_4$, 2 $\mu$g/ml aprotinin, and 50 ng/ml okadaic acid (pH 7.4). The cells were then immediately homogenized by 20 strokes with a motor-driven homogenizer in HES buffer containing 20 mM HEPES, 255 mM sucrose, 1 mM EDTA, 1 mM PMSF, 1 mM $Na_3VO_4$, 2 $\mu$g/ml aprotinin, and 50 ng/ml okadaic acid (pH 7.4) at 4 C. The homogenates obtained from two 10-cm diameter dishes per condition were subjected to subcellular fractionation to isolate the plasma membrane, cytosol, and nucleus as described previously (24). In brief, the homogenates were centrifuged at 19,000 × *g* for 20 min. The resulting supernatant was centrifuged at 250,000 × *g* for 90 min. The remaining supernatant was centrifuged at Centricon-30 (Amicon, Inc., Beverly, MA) and used as cytosol. The pellet obtained from the initial spin was resuspended in HES buffer, layered onto a 1.12-M sucrose cushion, and centrifuged at 100,000 × *g* in a swing rotor for 60 min. A white fluffy band at the interface was collected, resuspended in HES buffer, and centrifuged at 40,000 × *g* for 20 min, yielding a pellet of plasma membrane. A viscous brown pellet was collected, yielding a pellet of nucleus. The purities of the nuclear and cytosolic preparations were determined by examining histone as a nuclear marker and calpain as a cytosolic marker. The samples were adjusted to a final protein concentration of 1–3 mg/ml, which was measured by the Bradford method, and stored at −80 C before use.

### *Immunoprecipitation and Western blotting*

The cells or cell preparations were lysed in a buffer containing 30 mM Tris, 150 mM NaCl, 10 mM EDTA, 1% Nonidet P-40, 1 mM PMSF, 1 mM $Na_3VO_4$, 50 nM sodium fluoride, 10 $\mu$g/ml aprotinin, and 1 $\mu$M leupeptin (pH 7.4) for 30 min at 4 C. The lysates were centrifuged to remove insoluble materials. The supernatants (100 $\mu$g protein) were immunoprecipitated with antibodies for 16 h at 4 C. The immunoprecipitates or total cell lysates were then separated by 7.5% or 15% SDS-PAGE and transferred onto polyvinylidene difluoride membranes (Millipore Corp., Bedford, MA) using a Bio-Rad Transblot apparatus. The membranes were blocked in a buffer containing 50 mM Tris, 150 mM NaCl, 0.1% Tween 20, and 2.5% BSA or 5% nonfat milk (pH 7.5) for 2 h at 20 C. They were then probed with antibodies for 2 h at 20 C or for 16 h at 4 C. After the membranes had been washed in a buffer containing 50 mM Tris, 150 mM NaCl, and 0.1% Tween 20 (pH 7.5), blots were incubated with a horseradish peroxidase-linked secondary antibody and subjected to enhanced chemiluminescence detection using ECL reagent according to the manufacturer's instruction (Amersham Biosciences, Indianapolis, IN) (25, 26). In each experiment, the intensity of the band derived from control cells was averaged and assigned a value of 1 arbitrary unit, and the intensities of all treated groups were expressed relative to this value.

### *Statistical analysis*

Experiments were separately conducted at least four times, and data are presented as the mean ± SE. *P* values were determined by ANOVA and Scheffé test. $P < 0.05$ was considered statistically significant.

## Results

### *Effect of E2 on insulin-stimulated glucose uptake*

We first examined the concentration-dependent effect of E2 on insulin-stimulated 2-DOG uptake in 3T3-L1 adipocytes (Fig. 1A). Insulin at 17 nM stimulated 2-DOG uptake by 6.5 ± 0.6-fold in 3T3-L1 adipocytes. Low concentrations of E2 further increased uptake. Insulin-induced 2-DOG uptake was increased 18.3 ± 3.6% by treatment with $10^{-8}$ M E2 compared with that without E2 treatment. Conversely, concentrations of E2 above $10^{-7}$ M inhibited insulin-stimulated 2-DOG uptake. After treatment with $10^{-5}$ M E2, insulin-induced 2-DOG uptake was decreased by 25.8 ± 3.7% compared with that without E2 treatment. Insulin stimulated 2-DOG uptake in a

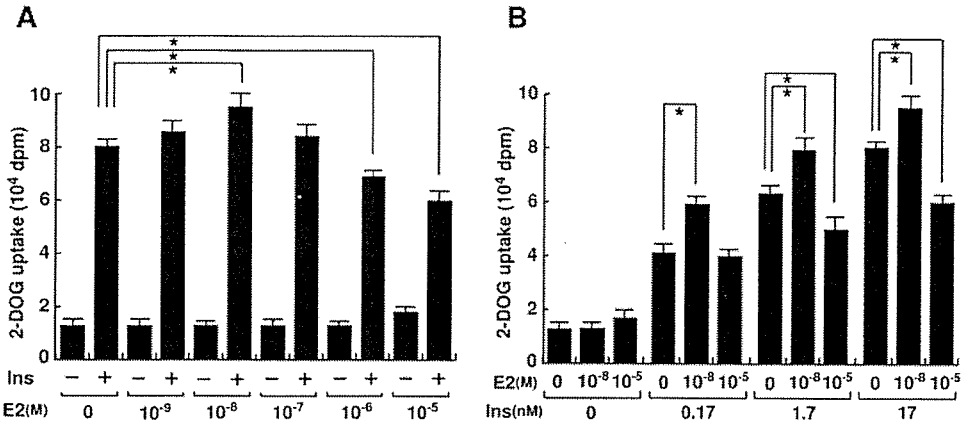


FIG. 1. Effect of E2 on insulin-induced 2-DOG uptake in 3T3-L1 adipocytes. A, Serum-starved cells treated with various concentrations of E2 for 16 h were then stimulated with 17 nM insulin for 15 min. B, Serum-starved cells treated with vehicle in ethanol, $10^{-8}$ M E2, or $10^{-5}$ M E2 were stimulated with various concentrations of insulin. Then the uptake of 2-[$^3$H]DOG for 4 min was studied. Each measurement was performed in duplicate, and results are the mean ± SE of seven separate experiments. *, $P < 0.05$ *vs.* 2-DOG uptake in control cells at the respective concentration of insulin without E2, by ANOVA and Scheffé's test.

concentration-dependent manner (Fig. 1B). Treatment with $10^{-8}$ M E2 significantly enhanced 0.17, 1.7, and 17 nM insulin-induced 2-DOG uptake, whereas $10^{-5}$ M E2 apparently inhibited 1.7 and 17 nM insulin-stimulated glucose uptake. E2 treatment alone for up to 16 h did not stimulate glucose uptake, and the amount of glucose transporter 4 was not altered by treatment with any concentration of E2 (data not shown).

*Effect of E2 on early steps of insulin signaling*

Because E2 affected insulin-stimulated glucose uptake, the possible involvement of E2 in the early steps of insulin signaling was examined. Insulin-induced tyrosine phosphorylation of the insulin receptor was not affected by treatment with E2 at any concentration (Fig. 2A). Interestingly, insulin-induced tyrosine phosphorylation of IRS-1 and the associa-

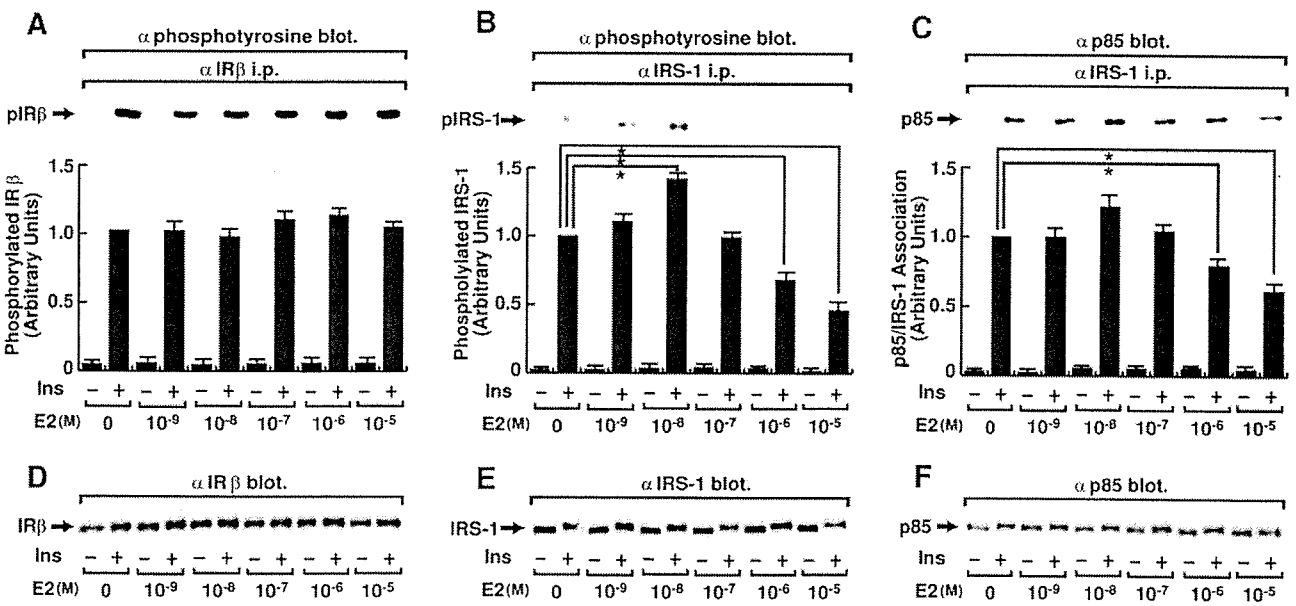


FIG. 2. Effect of E2 on early steps of insulin signaling. Serum-starved cells treated with various concentrations of E2 were stimulated with 17 nM insulin for 5 min. A, The cell lysates were immunoprecipitated with antiinsulin receptor antibody, and the precipitates were immunoblotted with antiphosphotyrosine antibody. B, The cell lysates were immunoprecipitated with anti-IRS-1 antibody, and the precipitates were immunoblotted with antiphosphotyrosine antibody. C, The cell lysates were immunoprecipitated with anti-IRS-1 antibody, and the precipitates were immunoblotted with anti-p85 antibody. Results are the mean ± SE of six separate experiments. *, $P < 0.05$ *vs.* insulin-induced phosphorylation of insulin receptor, phosphorylation of IRS-1, or association of p85 with IRS-1 in control cells stimulated with insulin in the absence of E2, by ANOVA and Scheffé's test. Total cell lysates were immunoblotted with antiinsulin receptor antibody (D), anti-IRS-1 antibody (E), or anti-p85 antibody (F).

tion of IRS-1 with the p85 subunit of PI3-kinase were promoted by treatment with a physiological concentration of E2. Thus, insulin-stimulated tyrosine phosphorylation of IRS-1 and IRS-1/p85 association were increased by 41.7 ± 3.4% and 22.9 ± 5.9%, respectively, after treatment with $10^{-8}$ M E2. In contrast, they were inhibited by treatment with concentrations of E2 above $10^{-7}$ M. At $10^{-5}$ M, E2 inhibited the insulin-induced tyrosine phosphorylation of IRS-1 and IRS-1/p85 association by 53.7 ± 3.7% and 25.9 ± 3.4%, respectively (Fig. 2, B and C). Amounts of protein among samples were confirmed to be equal by immunoblotting with antiinsulin receptor antibody (Fig. 2D), anti-IRS-1 antibody (Fig. 2E), and anti-p85 antibody (Fig. 2F).

*Effect of E2 on insulin-induced phosphorylation of Akt*

Akt lies downstream of PI3-kinase and is important for insulin's stimulation of glucose uptake (23, 27, 28). Because Akt is activated by phosphorylation at $Ser^{473}$ and $Thr^{308}$, we examined the effect of E2 on the insulin-induced phosphorylation of Akt (Fig. 3, A and B). Consistent with the results of insulin-induced tyrosine phosphorylation of IRS-1 and IRS-1/p85 association, insulin-induced phosphorylation of Akt was increased by treatment with low concentrations of E2 and decreased by treatment with high concentrations of E2. Insulin-induced phosphorylation of Akt at $Ser^{473}$ and $Thr^{308}$ was enhanced 22.0 ± 3.3% and 30.1 ± 3.2%, respectively, by treatment with $10^{-8}$ M E2, whereas it was inhibited 44.7 ± 3.5% and 50.8 ± 3.6%, respectively, by treatment with $10^{-5}$ M E2. Amounts of protein among samples were confirmed to be equal by immunoblotting with anti-Akt antibody (Fig. 3C).

*Effect of combined presence of E2 and TNF-α on insulin-stimulated tyrosine phosphorylation of IRS-1 and serine phosphorylation of Akt*

TNF-α together with estrogen are secreted from the placenta and are known to be involved in insulin resistance in the late phases of pregnancy, especially in preeclampsia (29, 30). The effect of combined presence of E2 ($10^{-6}$ M) and TNF-α on the insulin-induced tyrosine phosphorylation of IRS-1 and serine phosphorylation of Akt was examined. Insulin-induced tyrosine phosphorylation of IRS-1 was inhibited 24.6 ± 2.9% and 35.7 ± 3.6% by treatment with E2 and TNF-α, respectively (Fig. 4A). Insulin signaling was maximally inhibited by treatment with 50 ng/ml TNF-α. Treatment with both E2 and TNF-α further inhibited insulin signaling by 61.3 ± 4.2%. Similarly, treatment with E2, TNF-α, or both inhibited the insulin-induced phosphorylation of Akt by 21.8 ± 3.3%, 34.9 ± 3.0%, and 65.4 ± 3.3%, respectively (Fig. 4B). These results indicate that TNF-α combined with a submaximal concentration of E2 further inhibit insulin signaling, leading to glucose uptake.

*Effect of E2 on insulin-induced serine phosphorylation of IRS-1*

E2 affected insulin signaling at least at the level of tyrosine phosphorylation of IRS-1. Because tyrosine phosphorylation of IRS-1 is modulated by serine phosphorylation of IRS-1

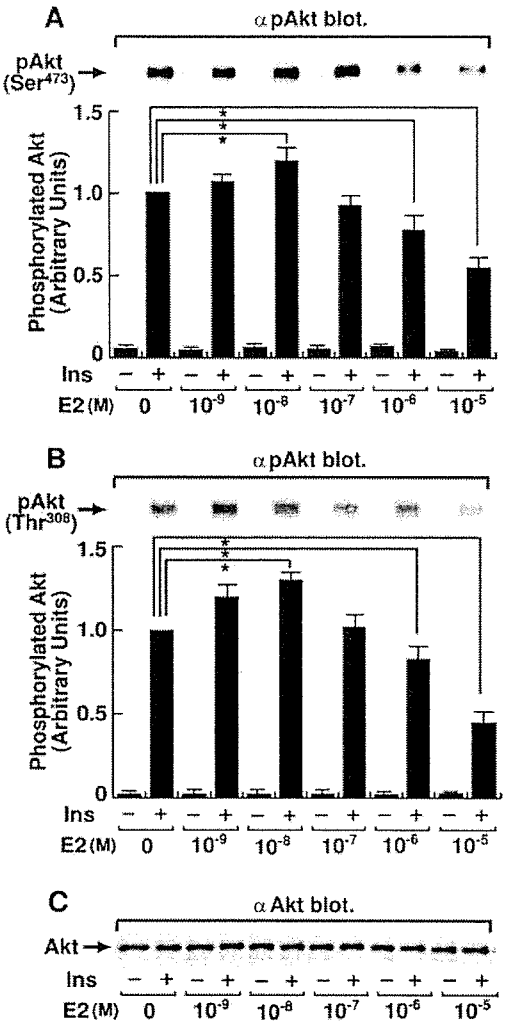


FIG. 3. Effect of E2 on insulin-induced phosphorylation of Akt. Serum-starved cells treated with various concentrations of E2 were stimulated with 17 nM insulin for 5 min. The cell lysates were immunoblotted with antiphospho-$Ser^{473}$-specific Akt antibody (A), antiphospho-$Thr^{308}$-specific Akt antibody (B), or anti-Akt antibody (C). Results are the mean ± SE of four separate experiments. *, $P < 0.05$ *vs.* insulin-induced phosphorylation of Akt without E2 treatment, by ANOVA and Scheffé's test.

(31), we examined the effect of E2 on the insulin-induced serine phosphorylation of IRS-1 (Fig. 5). The insulin-induced phosphorylation of IRS-1 at $Ser^{307}$ was increased by treatment with E2 in a concentration-dependent manner. The extent of phosphorylation at $Ser^{307}$ was increased 73.9 ± 4.1% by treatment with $10^{-5}$ M E2 (Fig. 5A). In contrast, the insulin-induced phosphorylation of IRS-1 at $Ser^{612}$ (Fig. 5B) and $Ser^{636}$ (Fig. 5C) was not altered by treatment with E2. These results indicate that a high concentration of E2 inhibits insulin signaling at the level of IRS-1 at least in part by increasing the phosphorylation of IRS-1 at $Ser^{307}$.

*Effect of a JNK inhibitor on the alteration of insulin signaling caused by E2 treatment*

Because IRS-1 is known to be phosphorylated by JNK at $Ser^{307}$ (32), we examined the influence of a JNK inhibitor,